AN OPTICALLY PUMPED IODINE LASER AMPLIFIER

by

MARTYN KENNETH BILLING

B.Sc., The University of British Columbia, 1976

A THESIS SUBMITTED IN PARTIAL FULFILMENT OF
THE REQUIREMENTS FOR THE DEGREE OF
MASTER OF SCIENCE

in

THE FACULTY OF GRADUATE STUDIES
DEPARTMENT OF PHYSICS

We accept this thesis as conforming
to the required standard

THE UNIVERSITY OF BRITISH COLUMBIA
January 1980

In presenting this thesis in partial fulfilment of the requirements for an advanced degree at the University of British Columbia, I agree that the Library shall make it freely available for reference and study. I further agree that permission for extensive copying of this thesis for scholarly purposes may be granted by the Head of my Department or by his representatives. It is understood that copying or publication of this thesis for financial gain shall not be allowed without my written permission.

Department of PHYSICS

The University of British Columbia
2075 Wesbrook Place
Vancouver, Canada
V6T 1W5

Date 21 JAN 1979

A B S T R A C T

The design process of an optically pumped amplifier for a CF_3I photodissociation laser is described.

In particular, a preamplifier is designed to amplify a 100 mJ laser pulse of 1 ns. duration which, by natural divergence, is contained in a beam of 2.5 cms diameter.

Experimental studies of the sub-system of this preamplifier and the associated diagnostics are described.

The operation of the preamplifier as part of the total laser system is discussed and suggestions are offered for the ongoing development of the device at the University of British Columbia.

TABLE OF CONTENTS

LIST OF FIGURES

Figure Page

LIST OF TABLES

CHAPTER I INTRODUCTION

In 1938 Porret and Goodeve published a theoretical paper in which they demonstrated that the photolysis of alkyliodes should produce iodine atoms mainly in the excited $2P^2_{\frac{1}{2}}$ state (1). Stimulated emission to the $2P^2_{3/2}$ ground state was first observed and reported by Kasper and Pimentel in 1964 (2).

In 1966 the first attempts to model the kinematic processes occurring during the photolysis and subsequent lasing were made, (3) and in 1967 scaling laws were derived which predicted that the iodine laser could be used to produce large output power pulses (4).

The first systematic study of the iodine laser began at the Institute of Plasma Physics (IPP), Garching, F.R.G., in 1970 and by 1972, motivated by the need for high power laser

pulses for fusion experiments, the decision was made to develop an 1KJ-1ns device. This laser, called Asterix III (5) is now operational and a schematic diagram of the major components is shown in Figure 1.

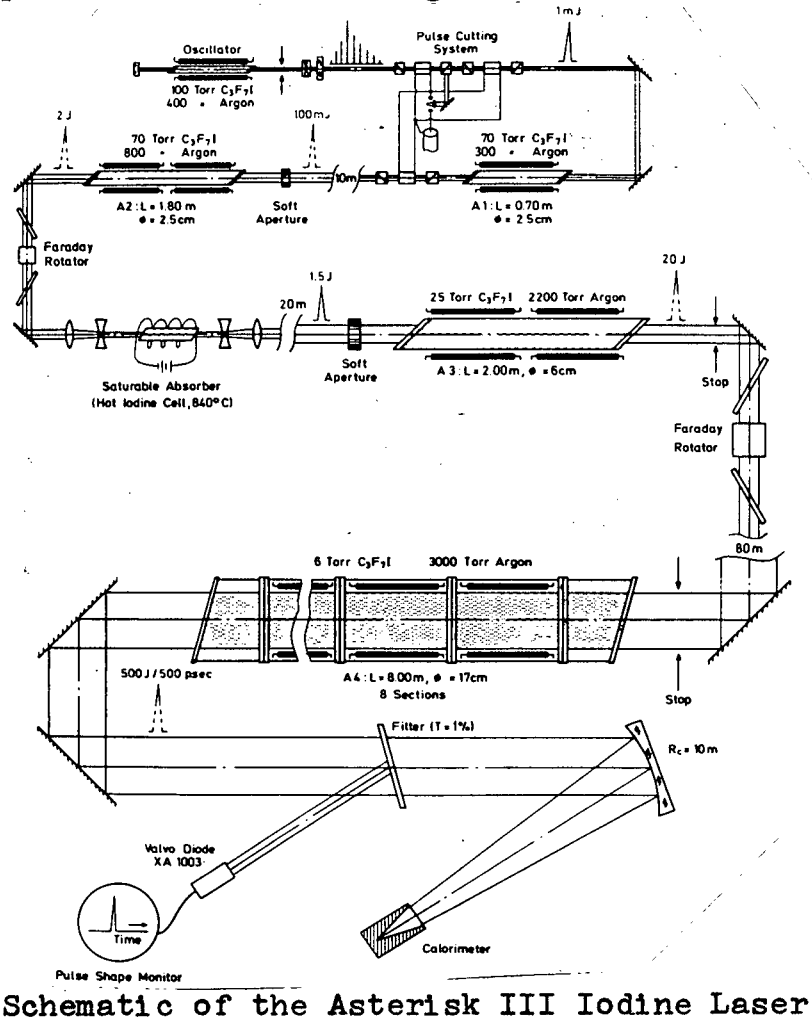

Fig. 1. Schematic of the Asterisk III Iodine Laser.

The acousto-optically mode locked oscillator has an active volume 1 cm. in diameter and 1 m. long and is operated in the gain switched mode. A pulse cutting system separates out a 1KJ-1ns pulse for amplification by the four subsequent stages. The energy in the output pulse of the

entire system is derived mainly from the final amplifier which has an active volume 20 cms. in diameter and 10 m. long. The alkyliodide (C_3F_7I) is optically pumped using 64 Xenon flash tubes, each 1 m. long.

Three pre-amplifier stages with diameters chosen to accomodate the natural divergence of the beam are used to raise the energy density to a level sufficient to release the stored energy in the final amplifier. Faraday rotators and a saturable absorber are included to improve the optical isolation of the individual stages. The repetition rate of the Asterisk III is limited to one shot each eight minutes by the gas recycling system which "cleans" the used gas and automatically delivers a new charge.

A terawatt iodine laser is also being developed at the Sandia Laboratories, Albuquerque, New Mexico (6). These gas laser systems have certain advantages over high power solid state devices:

1. Large geometric dimension of the active medium can be achieved more easily and cheaply.
2. Unlike solid state devices, the final amplifier of a gas laser system may be operated in saturation.

The broad line width of the laser transition in solid state materials results in the saturation energy density of an amplifier exceeding the damage threshold for the medium.

However, gas lasers, having narrow line widths, may be operated in saturation, thereby achieving a much improved extraction ratio. The line profile may be controlled by pressure broadening and the effect to optimize the operation of the device.

3. An improved beam quality is possible since local perturbations in the optical properties of the medium, typical of glasses, do not occur.

An iodine laser is under construction at the University of British Columbia, primarily for the use in laser-plasma interaction experiments. During the construction phase careful studies of the various subsections are being undertaken in order to generate a technical expertise within the department and contribute to the technical development of the device. At present, a fog cell optical isolater is being evaluated.

To this time an oscillator stage has been built and a preamplifier with an active volume 1 cm. in diameter and 1 m. long is under construction. This paper describes the design procedure for a gas laser amplifier stage, and in particular the design of a preamplifier for a 100 mJ-Ins laser pulse contained in a beam of diameter approximately 2.5 cms. is presented.

CHAPTER II

THE MAJOR COMPONENTS OF A GAS LASER AMPLIFIER

A schematic diagram of the major components of an optically pumped gas laser amplifier is shown below.

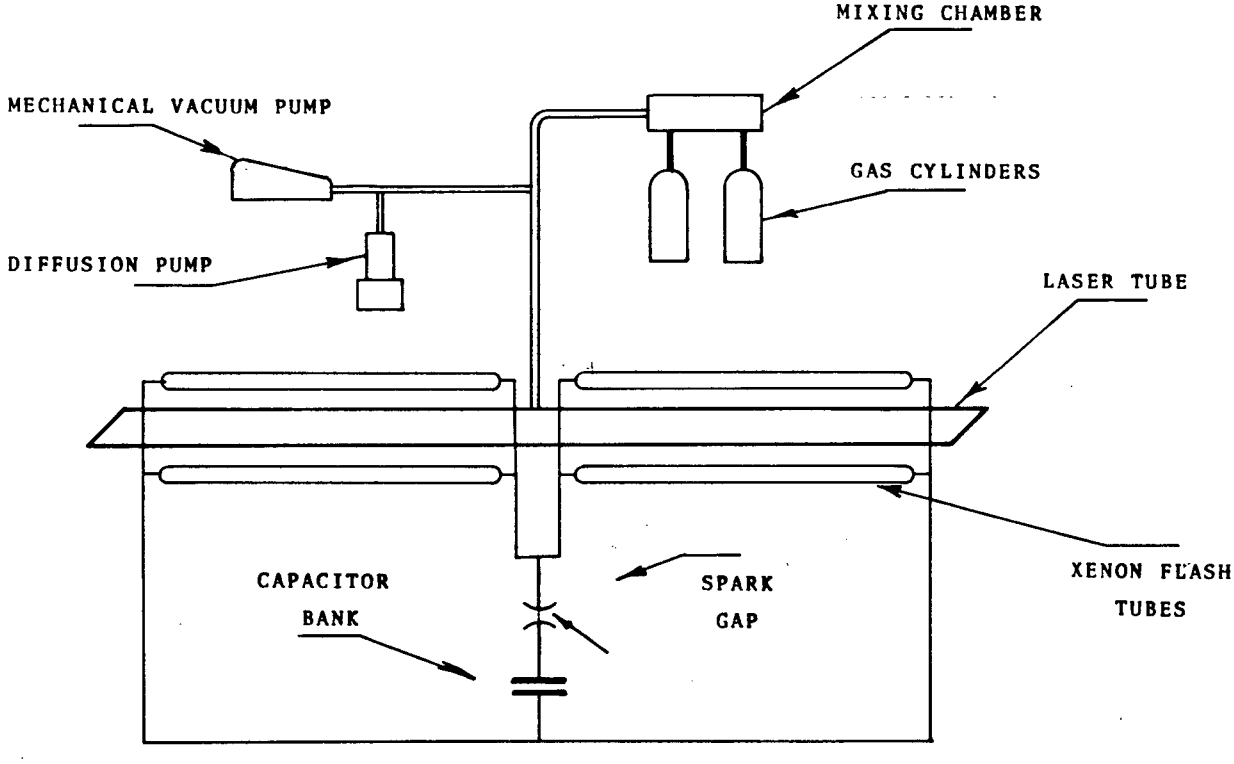

Fig. 2. Schematic Diagram of an Optically Pumped Gas Laser Amplifier.

The active medium is contained in a doped quartz tube and optical pumping is achieved using high intensity short pulse xenon flash tubes which are driven by a low inductance capacitor bank, the current being switched with a spark gap triggered by an S.C.R. unit. An active and a buffer gas are mixed in the manifold chamber before being passed to the laser tube. The gas system is evacuated by a mechanical and a diffusion pump.

CHAPTER III

THE SYSTEM DESIGN PROCESS

The objective of the system design process is to define the choice of component parts and their assembly into the complete device, together with the operating conditions, to achieve a specified system performance (Fig. 3).

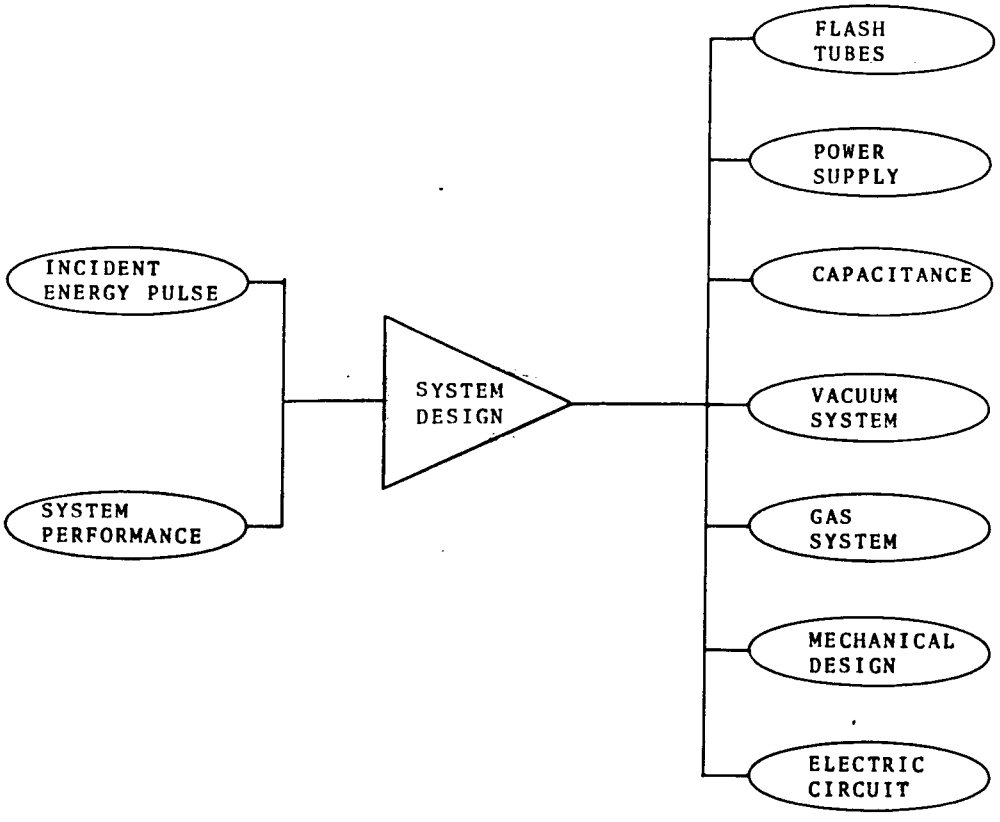

Fig. 3. The System Design Process

The system performance of an iodine amplifier can be specified in terms of seven parameters.

1. Gain: the total increase in energy of an incident pulse on passing through the amplifier.

2. Bandwidth: characterizing the frequency dependence of the system gain.

3. Extraction Ratio: the ratio of the stored energy to the energy extracted by the incident laser pulse.

4. Beam Quality: the spatial coherence and intensity profile of the beam should not be disturbed by the amplifier.

5. Efficiency: the ratio of the energy stored in the capacitor to the energy extracted from the active medium by the incident laser pulse.

6. Lifetime: the lifetime of the flash tubes.

7. Simplicity of Maintenance: (see Chapter 5).

In practice the design process cannot proceed as illustrated in Figure 3. Rather, the device design and the operating conditions are chosen and the system performance is then evaluated. Changes are made in the design or operating condition until the required system performance is achieved (see Figure 4).

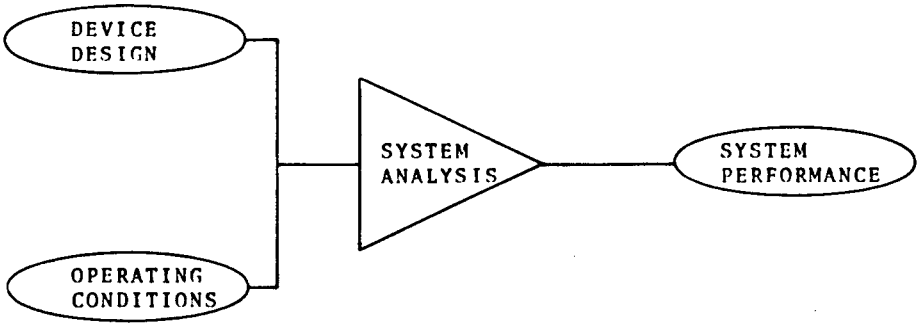

Fig. 4. The Systems Analysis Process.

The interrelations between the system performance, device design and operating conditions can be represented schematically on a Polya-Fuller map (Figure 5), where system variables are represented by ellipses and the relationship between the variables by squares. This diagram indicates clearly the complicated interdependence of the different design choices and performance criteria.

In order to be able to proceed with the design process, these relationships must be found explicitly.

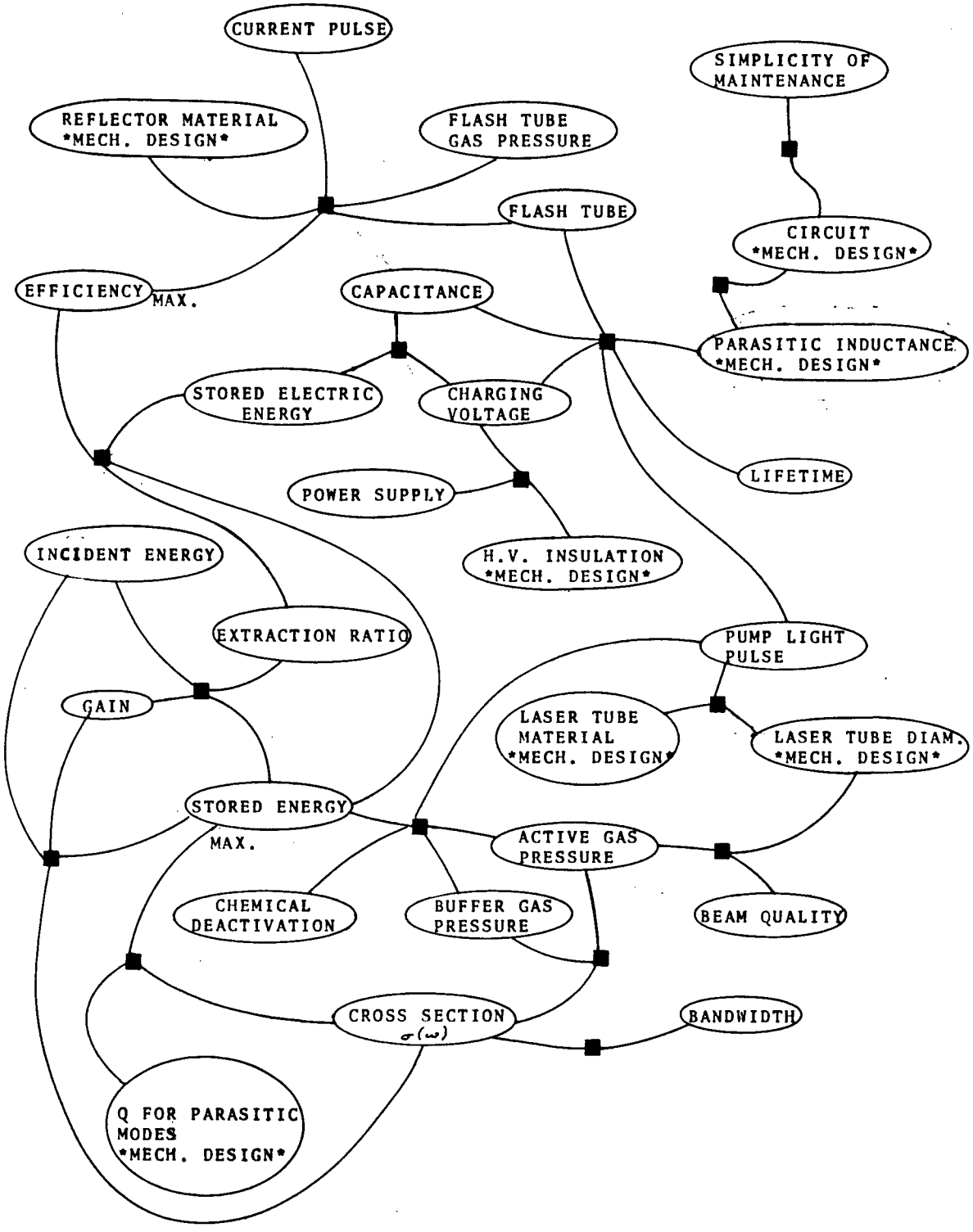

Fig. 5. System Design Relationships.

CHAPTER IV SYSTEMS ANALYSIS

A detailed analysis of the iodine laser system is presented in this chapter and the functional relationships as represented on the Polya-Fuller map are derived.

CHAPTER IV SECTION 1
THE PHOTOLYSIS OF CF_3I

The absorption spectrum of CF_3I, which is both Doppler and pressure broadened, has a maximum at 4.6 eV (2660A°) associated with the processes

$$CF_3I \xrightarrow{\hbar\omega} CF_3 + I(5P^2_{\frac{1}{2}}), \quad CF_3I \xrightarrow{\hbar\omega} CF_3 + I(5P^2_{3/2}) \qquad (1)$$

The cross-section for producing ground state ($5P^2_{3/2}$) is small (7) and hence this process may be ignored.

Breaking the C-I bond requires an energy of 2.46 eV and an additional 0.95 eV excites the iodine atom into the $2P^2_{3/2}$ state (8). The remaining 1.45 eV ultimately contributes to the heating of the entire gas.

CHAPTER IV SECTION 2

THE LASER TRANSITION

Lasing occurs between the $5P^2_{\frac{1}{2}}$ excited state and the $5P^2_{3/2}$ ground state of atomic Iodine. The excited and the ground states have degeneracies of 2 and 4 respectively and the transition has a radiative lifetime of 170 ms. (9). The iodine nucleus has a total angular momentum of $J_N=5/2$ (natural occurrence 100% ; (10)) and hyperfine splitting is observed. (See figures 6 and 7)

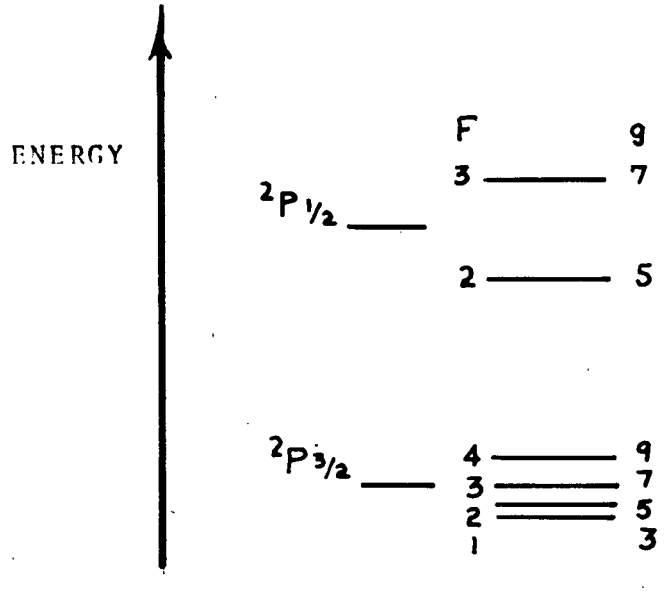

Fig. 6. The energy levels and degeneracies g of the Eigenstates of total angular momentum of the nucleus plus the electrons (quantum number F) of atomic iodine.

CHAPTER IV SECTION 2.1

THE SPECTRUM OF THE TRANSITION

The spectrum of the energy levels at a pressure of 15 Torr has been measured by Jaccarino (11) and is shown in Figure 7.

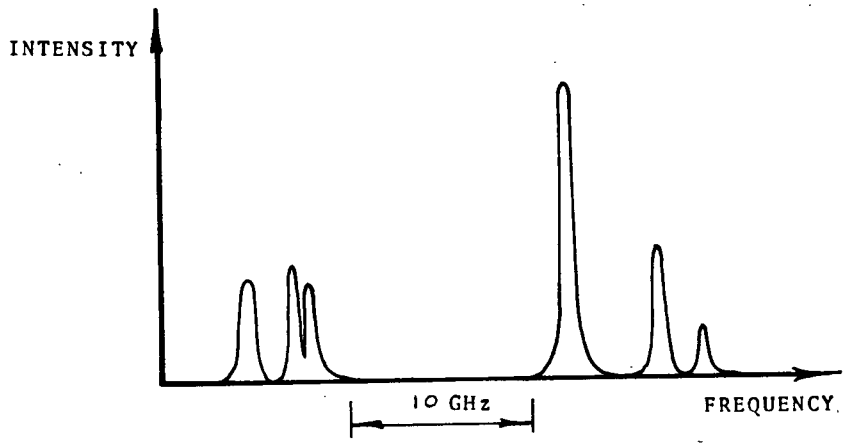

Fig. 7. The spectrum of the $5P^2_{\frac{1}{2}} - 5P^2_{3/2}$ transition, showing the hyperfine splitting due to the angular momentum and the quadrapole moment of the electric field of the nucleus.

The rate of stimulated emission S(w) into the frequency interval w to w+dw may be expressed either in terms of a frequency dependent inversion n(w) and a constant cross-section σ

$$S(w) = \sigma(w) \times \text{flux} \times n(w) \qquad (2)$$

or in terms of a frequency dependent cross-section $\sigma(w)$ and total inversion n

$$S(w) = \sigma(w) \times \text{flux} \times n \qquad (3)$$

Under the assumption that the occupation of the lower energy levels is small, the graphs of $\sigma(w)$ and $n(w)$ take the same form as figure 7.

CHAPTER IV SECTION 2.2

PRESSURE BROADENING

Pressure broadening often results in a Lorentzian line shape such that $\sigma(w)$ for a single transition is given by

$$\sigma(w) = 2\pi^2 \frac{Ac^2}{w^2} \frac{f(w-w_o)}{\Delta w_o} \qquad (4)$$

where

w_o is the resonant frequency of the transition
Δw_o is the half width
A is the Einstein coefficient for spontaneous emission between the upper and lower energy levels

and

$$f(w-w_o) = \left\{1 + \left[\frac{2(w-w_o)}{\Delta w_o}\right]^2\right\}^{-1} \qquad (5)$$

Since the half width varies directly with pressure the cross-section $\sigma(w)$ of each transition can be plotted for different degrees of pressure broadening. CO_2 or Argon may be added to the active gas to achieve this broadening, the broadening coefficients being 9MHz per Torr (12) and 4.5 MHz per Torr respectively (13, 12). Calculations by K. Hohla (5) show that at a buffer pressure of 400 Torr CO_2, the total cross-section $\sigma(w)$ for a transition between the

upper and lower energy levels has merged into a single line. At this pressure the frequency roll off due to the limited bandwidth will not significantly broaden a laser pulse of 1 ns. duration as it passes through an amplifier (14). Similarly, a buffer pressure of 2000 Torr Argon is sufficient for a 200 ps. pulse (6).

CHAPTER IV SECTION 2.3
EFFECTIVE CROSS-SECTION

In the analysis of Sections 2.3 and 2.4 of this chapter, it is convenient to describe the rate of change of photon density within the radiation field due to stimulated processes by the equation

$$\frac{dq}{dt} = \sigma_E \, c \, q(t) \, n(t) \qquad (6)$$

where q is the total number of photons per unit volume within the radiation field, σ_E is an effective cross-section for the processes, c is the velocity of light and n is the total inversion per unit volume.

If such a model is to be used, then the line shape of the radiation field and the gain profile of the laser medium must be accounted for within the effective cross-section σ_E. An expression for σ_E will now be derived.

The rate of change of the number of photons in a unit volume within the radiation field is given by

$$\frac{dq}{dt} = B_{12}\, q\, n_1' - B_{21}\, q\, n_2' \qquad (7)$$

where n_1' is the total number of atoms in a unit volume that could emit a photon into the radiation field, n_2' is the total number of atoms in a unit volume that could absorb a photon from the radiation field and B_{12} and B_{21} are the Einstein coefficients for the transitions.

Using the relation

$$B_{12} g_1 = B_{21} g_2$$

we can write equation (7) in the form

$$\frac{dq}{dt} = B_{12}\, q(n_1' - g_1/g_2\, n_2') \equiv B_{12}\, q\, n' \qquad (8)$$

Restrict attention to the photons in the radiation field within one half width at full maximum of the spectral line (f(w)) then

$$q = \int_{w_-}^{w_+} f(w)\, dw \qquad (9)$$

and n' may be written as

$$n'(t) = n(t) \int_{w_-}^{w_+} \frac{G(w)}{\Delta w_0}\, dw \qquad (10)$$

Here, $G(w)$ is the line shape factor of the laser transition, Δw_o is the half width of the laser transition, w_o' is the central frequency of the radiation field spectrum, $\Delta w_o'$ is the half width of the radiation field spectrum and n is the total inversion per unit volume and $w_\pm = w_o' \pm w_o'$.

Substituting equation (10) into (9) we have

$$\frac{dq}{dt} = B_{12}\, q\, n \int_{w_-}^{w_+} \frac{G(w)}{\Delta w_o}\, dw \qquad (11)$$

Defining the effective cross-section to be

$$\sigma_E \equiv B_{12}/c \int_{w_-}^{w_+} \frac{G(w)}{w_o}\, dw \qquad (12)$$

we have as required

$$\frac{dq}{dt} = \sigma_E\, c\, q\, n \qquad (6)$$

There are two cases to consider. The homogeneously broadened line where $G(w)$ is not a function of time, and the inhomogeneously broadened line where $G(w)$ changes with time.

In a homogeneously broadened line the total number of atoms in energy Eigenstates which can emit a photon into the radiative field is maintained by a process sufficiently fast that the entire inversion is depleted by lasing. (See Figure 8)

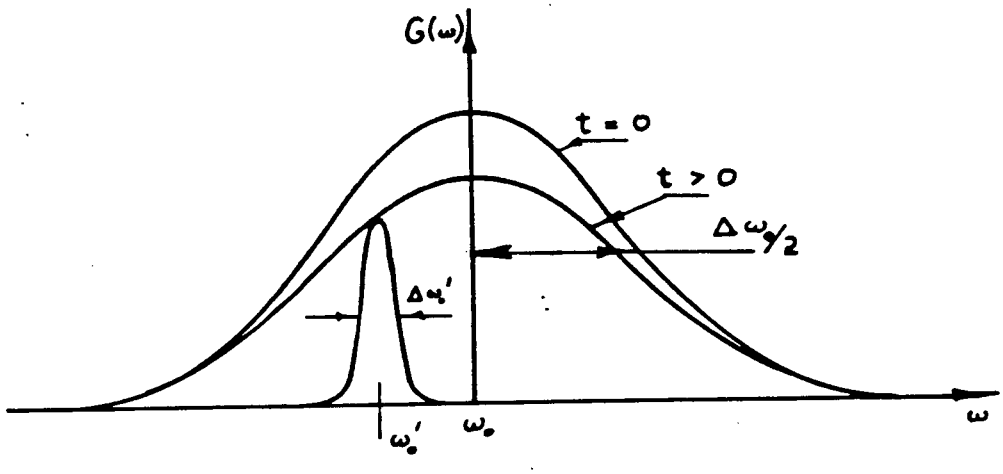

Fig. 8 The depletion of the inversion of an homogeneously broadened line.

An inhomogeneously broadened line exhibits hole burning whereby the atoms able to emit a photon into the radiation field are consumed faster than they can be replenished from other spectral regions of the transition, i.e., G(w) changes with time. (See Figure 9)

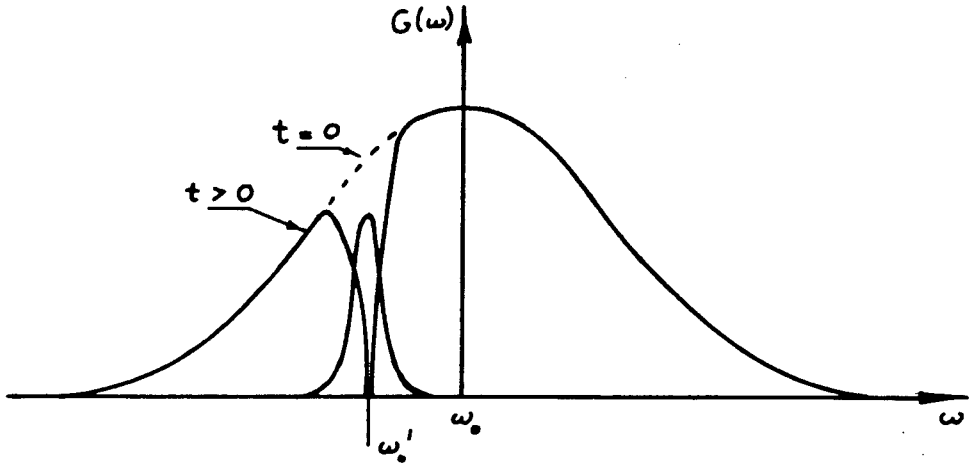

Fig. 9. The depletion of the inversion of an inhomogeneously broadened line.

Whether a transition is homogeneously or inhomogeneously broadened depends on the pulse duration of the radiation field. In the CF_3I laser the transition is Doppler and pressure broadened, and in both cases collisions between particles are responsible for the "diffusion" between spectral regions. The characteristic time, t_c, between collisions can be written

$$t_c = \frac{1}{n_o \; v \; \sigma_k} \tag{13}$$

where n_o is the total particle density, $\bar{v}$ is the mean thermal velocity and σ_k is the gas-kinetic collision cross-section.

Using values for the CF_3I laser of

$$n_o = 3 \times 10^{18} \quad (100 \text{ Torr})$$
$$\bar{v} = 2 \times 10^{4} \text{ cm/sec} \quad (400 \text{ K})$$
$$\sigma_k = 6 \times 10^{-15} \text{ cm}^2 \qquad (7)$$

we find

$$t_c \simeq 2 \times 10^{-9} \text{ s}$$

The radiation field in an oscillator stage exists for approximately 1μs., which is one order of magnitude greater than this characteristic time between collisions. Therefore, the transition may be treated as homogeneously broadened with time independent σ_E.

In an amplifier stage the bandwidth of the transition is chosen to accomodate the incident signal. Consequently, a short duration incident energy pulse will imply a large gas pressure and subsequently a short characteristic time between collisions. The transition may, therefore, again be modelled as being homogeneously broadened.

The relation between the effective cross-section, the pressure of the active gas and the pressure of the buffer gas for a 1 ns. laser pulse has been measured and presented graphically by K. Hohla et al (10).

CHAPTER IV SECTION 3

STORED ENERGY

The population inversion, created by the photolysis of CF_3I, is depleted by chemical and radiative processes. Excited iodine may react with the various by-products of the photolysis process or may decay spontaneously, or by stimulated emission, to the ground state.

CHAPTER IV SECTION 3.1

CHEMICAL DEACTIVATION

3.1.1. The Chemical and Photolytic Processes

The processes occurring in a gas mix, initially consisting of CF_3I and O_2, which is optically pumped, are:

1. Photolysis:

$$CF_3I + \hbar w \xrightarrow{K_1} CF_3 + I(5P^2_{\frac{1}{2}})$$

$$CF_3I + \hbar w \xrightarrow{K_2} CF_3 + I(5P^2_{3/2})$$

K_2 is small and consequently this process is ignored (7)

2. Recombination Processes:

$$I^* + CF_3 \xrightarrow{K_3} CF_3I$$

$$I + CF_3 \xrightarrow{K_4} CF_3I$$

3. Deactivation Processes:

a. Reactions of the form $I^* + M \xrightarrow{K_M} I + M$

i) $I^* + CF_3I \xrightarrow{K_5} I + CF_3I$

ii) $I^* + CF_3 \xrightarrow{K_6} I + CF_3$

iii) $I^* + C_2F_6 \xrightarrow{K_7} I + C_2F_6$

iv) $I^* + O_2 \xrightarrow{K_8} I + O_2$

v) $I^* + I_2 \xrightarrow{K_9} I + I_2$

These two particle encounters behave as first order reactions such that

$dn_c/dt = K\, n_A\, n_B$ for $A + B \xrightarrow{K} C + D$

b. Reactions of the form $I^* + I + N \xrightarrow{K_N} I_2 + N$

vi) $I^* + I + CF_3I \xrightarrow{K_{10}} I_2 + CF_3I$

vii) $I^* + I + I_2 \xrightarrow{K_{11}} 2I_2$

The reaction rates of these three particle encounters are of second order and are characterized by

$dn_{I_2}/dt = K(n_I + n_{I^*})^2\, n_N$

4. Dimerization of the CF_3I Radical:

$$2CF_3 \xrightarrow{K_{12}} C_2F_6$$

This is also a first order reaction. Estimated and measured coefficients are listed in reference ( ).

Notation:

n_{CF_3I}	$\equiv$	n_o	n_{I*}	$\equiv$	n_1	n_I	$\equiv$	n_2
n_{CF_3}	$\equiv$	n_3	$n_{C_2F_6}$	$\equiv$	n_4	n_{I_2}	$\equiv$	n_5
n_w	$\equiv$	n_6	n_{O_2}	$\equiv$	n_7			

3.1.2 The Rate Equations

The rate of change of the concentration of CF_3I depends on the following processes:

1. $CF_3I + \hbar w \xrightarrow{K_1} CF_3 + I^*$ $= dn_3/dt = K_1 n_o n_6$
   $= dn_o/dt = -K_1 n_o n_6$

2. $I^* + CF_3 \xrightarrow{K_3} CF_3I$ $= dn_o/dt = K_3 n_3 n_1$

3. $I + CF_3 \xrightarrow{K_4} CF_3I$ $= dn_o/dt = K_4 n_3 n_2$

Thus we have

$$dn_o/dt = -K_1 n_o n_6 + K_3 n_3 n_1 = K_4 n_3 n_2$$

Similarly

$$dn_1/dt = K_1n_on_6 - K_5n_on_1 - K_6n_1n_3 - K_3n_1n_3 - K_7n_1n_4 - K_8n_1n_7 - K_9n_1n_5 - K_{10}(n_1 + n_2)^2n_o - K_{11}(n_1+n_2)^2n_5$$

$$dn_2/dt = K_5n_on_1 + K_6n_1n_3 - K_4n_2n_3 + K_7n_1n_4 + K_8n_1n_7 + K_9n_1n_5 - K_{10}(n_1+n_2)^2n_o - K_{11}(n_1+n_2)^2n_5$$

$$dn_3/dt = K_1n_on_6 - K_3n_1n_2 - K_4n_2n_3 - K_{12}n_3^2$$

$$dn_4/dt = K_{12}n_3^2$$

$$dn_5/dt = K_3(n_1+n_2)^2n_o + K_4(n_1+n_2)n_5$$

$$dn_6/dt = P(t) - K_1n_on_6$$

where P(t) is the rate of change of photon density due to optical pumping

$$dn_7/dt = \quad - K_8n_1n_7$$

3.1.3. Dominant Deactivation Process

In order to achieve a complete understanding of the temporal behaviour of the population of I*, these rate equations must be solved numerically. However, some insight into the relative importance of the different deactivating processes may be gained by evaluating the half life of I* for each, using an estimate for the number density of the collision partner.

In general, for the bimolecular reaction

$$A + B \xrightarrow{K_M} C + D$$

the half life is

$$T_{\frac{1}{2}A} = -(\ln \tfrac{1}{2})/K_M n_B$$

and for the second order three body encounters considered

$$A + B + C \xrightarrow{K_M} C + D$$

the half life is

$$T_{\frac{1}{2}A} \simeq 1/2K_M n_B n_C$$

1. $I^* + CF_3I \xrightarrow{K_5} I + CF_3I$

   For 100 Torr CF_3I we have

   $T_{\frac{1}{2}I^*} \simeq 10^{-3}$ seconds

2. $I^* + CF_3 \xrightarrow{K_6} I + CF_3$

   $I^* + CF_3 \xrightarrow{K_3} CF_3I$

   By estimating the total energy emitted by the flash-lamps within the absorption spectrum of CF_3I, an upper bound of 10^{17} cms^{-3} is found for the concentration of the CF_3 radical. This then gives

   $T_{\frac{1}{2}I^*} \simeq 2.5 \times 10^{-6}$ seconds

---

where

$K_3 = 3.7 \times 10^{-12} s^{-1}$ $\quad$ $K_5 = 3 \times 10^{-16} s^{-1}$

$K_6 = 3.7 \times 10^{-12} s^{-1}$ $\quad$ $K_7 = 4.5 \times 10^{-16} s^{-1}$

$K_8 = 8.6 \times 10^{-12} s^{-1}$ $\quad$ $K_9 = 5 \times 10^{-12} s^{-1}$

3. $I^* + C_2F_6 \xrightarrow{K_7} I + C_2F_6$

K_7 has a value of 4.5×10^{-16} seconds^{-1} (10) and therefore the corresponding half-life of I* is long. C_2F_6 may be used as a thermal buffer since even for 100 Torr C_2F_6 we have

$T_{\frac{1}{2}I^*} \simeq 10^{-3}$ seconds

4. $I^* + O_2 \xrightarrow{K_8} I + O_2$

For a pressure of residual oxygen of 3×10^{-3} Torr

$T_{\frac{1}{2}I^*} \simeq 10^{-3}$ seconds

5. $I^* + I_2 \xrightarrow{K_9} I + I_2$

It is difficult to estimate the number density of I_2. However, since the rate coefficient for the reaction is 5×10^{-12} seconds^{-1} (10), it is clear that even small quantities will result in significant deactivation.

3.1.4. Concentration of Important Deactivating Species

We have thus found that the CF_3 radical and molecular iodine are the species primarily responsible for the deactivation of the excited iodine. It is not instructive to study the reactions which govern their populations.

The CF_3 radical, produced by photolysis, is eliminated in the following ways, with half life estimated as before.

$$2\ CF_3 \xrightarrow{K_{12}} CF_3I \qquad T_{\frac{1}{2}CF_3} \simeq 3 \times 10^{-6}\text{seconds}$$

$$I + CF_3 \xrightarrow{K_4} CF_3I$$

The population of ground state iodine is small (7) and thus the dimerization reaction governs the concentration of CF_3.

Similarly, for I_2 we have

$$I + I^* + CF_3I \xrightarrow{K_{10}} I_2 + CF_3I \qquad T_{\frac{1}{2}I_2} \simeq 10^{-4}\text{seconds}$$

$$I + I^* + I_2 \xrightarrow{K_{11}} 2\ I_2 \qquad T_{\frac{1}{2}I_2} \simeq 10^{-4}\text{seconds}$$

Thus only a small concentration of molecular iodine occurs during the duration of the pump pulse.

3.1.5. Thermal Effects

It is important to keep the gas mix cool since the rate coefficients and hence chemical deactivation increases with temperature. Also, thermal dissociation of CF_3I, which preferentially produces atomic iodine in the ground state (15) directly reduces the inversion.

Heating is primarily due to the dimerization of 2 CF_3 to C_2F_6 and the photolysis of CF_3I, yielding 3.66 and 1.45 eV per reaction respectively (16). A buffer gas, which will not chemically interact with CF_3I or subsequent by-products of the photolysis, may be used as a thermal reservoir.

3.1.6. Summary

For a gas mix with less than 3×10^{-3} Torr of residual oxygen, the dominant deactivating species are the CF_3 radical and molecular iodine. Both result in a significant loss of stored energy during a typical pump pulse (6-20 ns.).

CF_3 rapidly dimerizes to C_2F_6 and consequently is eliminated soon after the pump pulse has terminated.

A buffer gas may be added to absorb thermal energy, thereby keeping the chemical deactivation rate and the rate of thermal dissociation of CF_3I producing ground state iodine to a minimum.

CHAPTER IV SECTION 3.2
RADIATIVE DEACTIVATION

3.2.1. Parasitic Oscillations

Since the small signal gain of the laser medium is large the threshold conditions for oscillation in a cavity with low Q, typical of an amplifier, may be achieved. The energy loss due to these parasitic modes is so large that the threshold inversion turns out to be the upper limit of the stored energy (10).

1. Resonant Cavity Modes

Reflecting surfaces such as the laboratory walls and optical components together with dust particles which act as scattering centres may give rise to the lasing of cavity modes.

The threshold inversion is defined by the condition that the energy input into the mode due to stimulated and spontaneous emission is identical to the energy loss due to imperfect reflections and absorptions.

If q_o is the energy density at the first mirror with reflectivity R_1, then after one complete cycle through the cavity the energy density will be changed to

$$q = (q_o R_1 \; T \exp. \; \sigma_M \; n \; L)(R_2 \; T \exp. \; \sigma_M \; n \; L) \qquad (14)$$

where R_2 is the reflectivity of the second mirror, T is the transmittance of the medium in the cavity and σ_M is the effective cross-section for stimulated emission into the mode.

For a mode which grows in time we have

$$R_1 \; R_2 \; T^2 \exp. \; 2 \; \sigma_M \; n \; L \geqslant 1 \qquad (15)$$

From this we see that the threshold inversion

$$N_T \equiv nL_{\text{THRESHOLD}} = \frac{\ln \; (1/R_1 R_2 T^2)}{2 \; \sigma_M} \qquad (16)$$

This condition may also be expressed in terms of the quality factor Q of the cavity defined by the differential equation

$$dq/dt = (-w_o/Q)\ q \tag{17}$$

where $1/w_o$ is the time taken for the energy pulse to make a round trip to the cavity.

Rearranging equation 17 and integrating over one cycle denoted $0 \leq t \leq T$, we have

$$\text{Ln } q(T) - \ln q(o) = (-w_o/Q)\ T = -1/Q$$

$$\Rightarrow\ Q = \frac{1}{\ln(q(o)/q(T))} \tag{18}$$

Evaluating this in terms of the cavity parameters we find

$$Q = \frac{1}{\ln(1/R_1 R_2 T^2)} \tag{19}$$

Thus, using this in equation 17 the threshold inversion, or maximum stored energy, is given by

$$N_T = 1/2Q\sigma_M \tag{20}$$

2. Guided Wave Modes

Oscillations which grow in time also occur due to reflections from the laser tube wall or the flash tube reflectors.

For large angles of incidence θ the wave is predominantly reflected at the surface of the quartz laser tube and therefore travels exclusively in the activated laser medium (see Figure 10). This results in a large Q value and consequently a low threshold inversion.

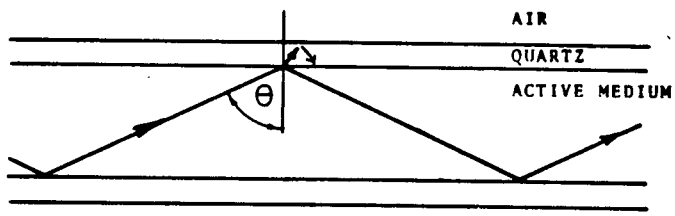

Fig. 10. Guided wave mode confined within the laser tube since the angle of incidence θ is large.

Although rays incident at small angles are transmitted into the non-activated region, the increased number of bounces before the wave leaves the amplifier can also result in a significant amount of energy being extracted. (See Figure 11)

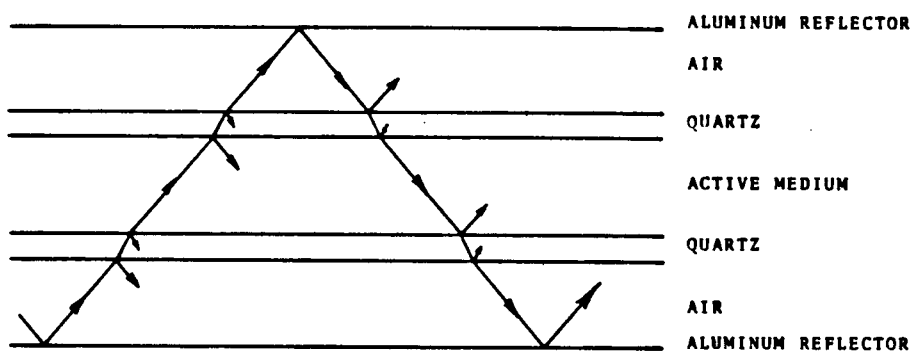

Fig. 11. Guided wave modes typical of small incident angles, the wavefront being confined by the flash tube reflector.

Rays at large angles of incidence may be suppressed by inserting an aluminum coil against the inner surface of the laser tube such that they are reflected and coupled into more lossy modes (17).

Parasitic modes with frequency near the laser line centre have the lowest threshold and are therefore the most troublesome. The cross-section at the line centre may be lowered by pressure broadening and hence the maximum stored energy increased.

Ruby and Nd-glass have a maximum cross-section of approximately 10^{-20}cms^2 (16) and thus can achieve a stored energy density an order of magnitude greater than iodine, which has a value in the range 2 - 5 x 10^{-19} cms^2.

An energy density of 6 J/cms^2 is possible in iodine with σ_{MAX} reduced to 2 x 10^{-19}cms^2 by pressure broadening. D. Gregg et al suggest that additional broadening may be achieved by using the Zeeman effect (18).

3.2.2. Optical Coupling Losses

Prepulses generated by super radiance result in a serious energy loss as they pass through the amplifier chain.

A saturable absorber, as developed at the IPP, Garching, may be used to isolate each amplifier stage. However, the device is elaborate and still in the early stages of its development (19).

The super radiant field is less directional than the laser beam and hence a reasonable degree of isolation may be achieved by separating the stages by a large distance. This does not require any compromise in the design of a final amplifier since the large beam diameter and energy density define a distance between the stages which is sufficient to provide good isolation. However, initially the natural divergence of the narrow laser beam results in an energy density below that required to saturate an amplifier, even for a separation distance required for a minimum isolation.

If this method of optical isolation is used then one of two design compromises must be made.

1. The buffer gas pressure may be lowered, thereby reducing the saturation energy and improving the extraction ratio. The reduced bandwidth will result in some broadening of the laser pulse and lower buffer pressure results in a smaller maximum stored energy.

2. The buffer gas pressure may be chosen to provide adequate bandwidth and maximize the stored energy. The resulting poor extraction ratio must be accepted.

CHAPTER IV SECTION 3.3.

THE TEMPORAL BEHAVIOUR OF THE STORED ENERGY DUE TO THE ONSET OF PARASITIC OSCILLATIONS

The time evolution of the energy in an axial mode of a resonant cavity containing an activated medium is studied.

The rate of change of the total number of photons per unit area U_M in the mode is given by

$$dU_M/dt = fAN_1' + \sigma_M (cU_M/L)\Delta N - cU_M/2QL \qquad (21)$$

where N_1' is the total number of particles which could emit a photon into the mode, N is the total inversion, f is the fraction of the spontaneously emitted photons which are emitted in the direction of the cavity axis, A is the Einstein coefficient for the spontaneous emission process, c is the velocity of light, σ_E is the effective cross-section for the mode, Q is the quality factor of the cavity and L is the distance between the mirrors in centimeters.

The first term on the left-hand side of equation (21) describes the energy change due to spontaneous emission.

The second term characterizes the stimulated radiative processes and the third describes the power loss due to imperfections in the cavity.

The population of the upper level (N_1) is decreased by chemical deactivation, spontaneous and stimulated emission and increased by pumping such that

$$dN_1/dt = P_1(t) - \sigma_M(c/L)U_M\Delta N - AN_1 \qquad (22)$$

Similarly

$$dN_2/dt = P_2(t) + \sigma_M(c/L)U_M\Delta N + AN_1 \qquad (23)$$

where $P_1(t)$ denotes the rate of change of the population of the i-th energy level due to both pumping and chemical deactivation.

The system of equations 21, 22 and 23 have been solved numerically by K. Hohla et al (16) for the conditions typical of the Iodine laser oscillator (Figure 12).

I.e. $\Delta w_o = 5 \times 10^9$ Hz

$R_1R_2T^2 = 0.3$

$P_2(t)$ was taken to be zero.

The form of this solution is also appropriate for the transient behaviour of the parasitic modes of an amplifier stage.

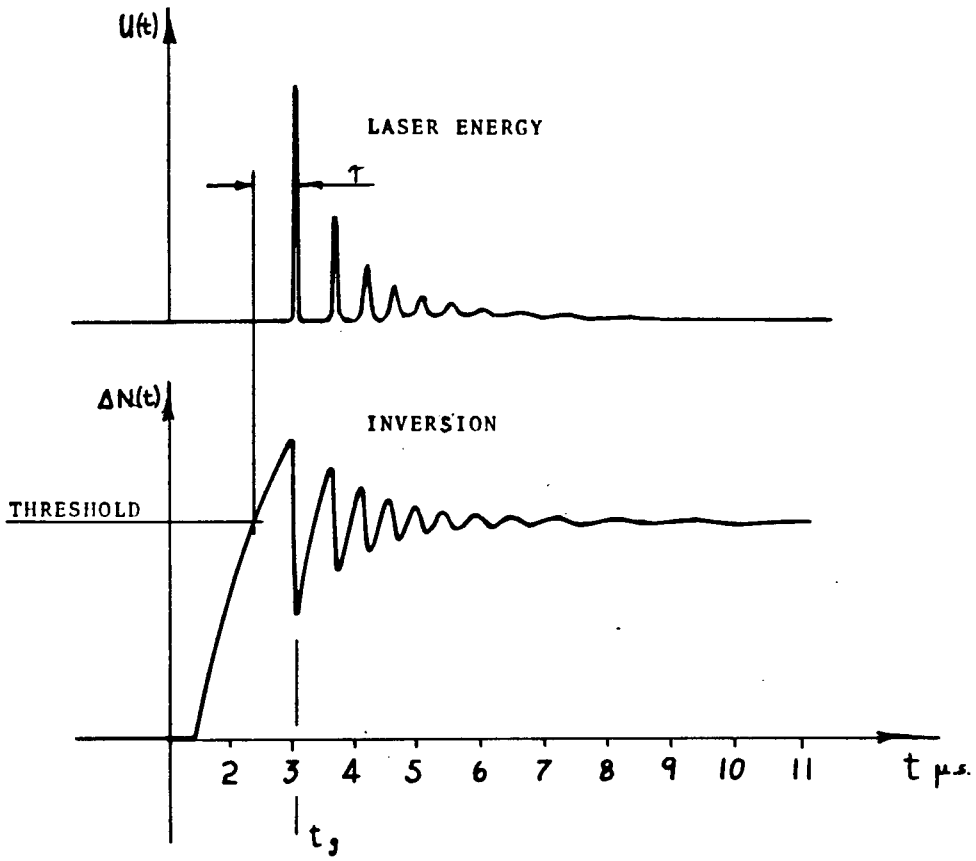

Fig. 12. The transient behaviour of the inversion and the resulting laser energy due to a pump light pulse initiated at t = 0.

CHAPTER IV SECTION 3.4

INERTIAL DELAY

The interval between the inversion reaching threshold and the full development of the laser pulse is referred to as the inertial delay of the system and may sometimes be used to advantage. (See Figure 12)

This delay can be understood quantitatively by examining the dominant terms in the rate equations for the interval near the threshold.

Equation 21 reduces to

$$dU_M/dt = \sigma_M (c/L) U_M \ \Delta N(t) \qquad (24)$$

For ΔN constant, this has solution

$$U_M(t) = U_o \exp. \ \sigma_M (c/L) \Delta N(t) \qquad (25)$$

However, ΔN is increasing due to pumping and hence the rate of change of $U_M(t)$ will increase with time. (See figure 13)

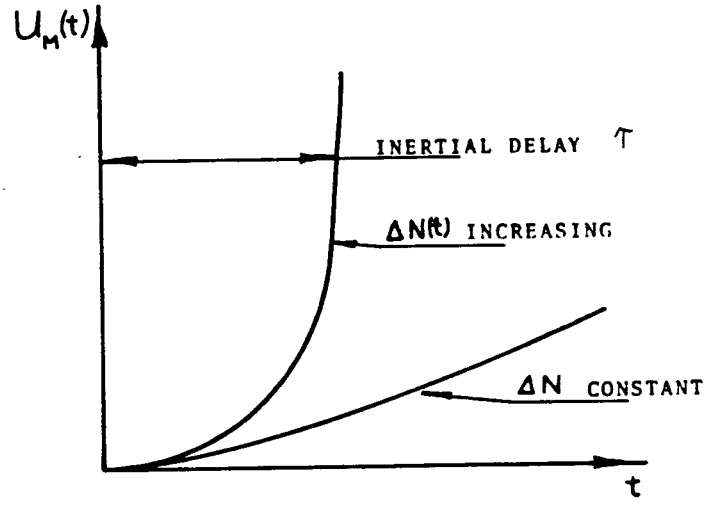

Fig. 13. The inertial delay of a laser pulse generated in a resonant cavity.

The amount of energy delivered in the first pulse will depend upon the total number of atoms which can be pumped

to the upper state before the rapid growth of the laser pulse occurs. If pumping is terminated at t_g, as shown in figure 12, then all of the energy is contained within the first laser pulse. Rapid pumping can therefore be used to eliminate the need for Q switching a laser oscillator (20) and in an amplifier stage it is possible to exceed the threshold for parasitic oscillations and therefore increase the maximum stored energy.

Inertial Delay in an Amplifier Stage

The inertial delay of an amplifier stage could be used to advantage if an inversion significantly greater than the threshold for parasitic oscillations could be achieved. The small signal gain and consequently the extraction ratio as well as the overall gain of the amplifier would be improved.

In order to evaluate the ratio of the maximum stored energy to the threshold inversion in an amplifier, approximate expressions for the inertial delay and the maximum inversion are derived from solutions of the rate equations.

The following simplifying assumptions are made:

1. The pump rate P is constant.
2. Chemical deactivation can be ignored.
3. Spontaneous emission can be ignored.

Then equations 21, 22 and 23 become

$$dU_n/dt = \sigma_M (c/L) U_M \Delta N - (c/2QL) U_M \tag{26}$$

$$dN_1/dt = P - \sigma_M (c/L) U_M \Delta N \tag{27}$$

$$dN_2/dt = \sigma_M (c/L) U_M \Delta N \tag{28}$$

From equations 27 and 28 we find

$$d/dt(N_1 - (g_1/g_2) N_2) = P - (1+g_1/g_2)\sigma_M (c/L) U_M \Delta N$$

$$\text{i.e. } d\Delta N/dt = P - b\, \sigma_M (c/L) U_M \Delta N \tag{29}$$

$$\text{when } b = (1 + g_1/g_2) \tag{30}$$

Initially, when the inversion is small

$$P \gg b\, \sigma_M (c/L) U_M \Delta N \tag{31}$$

and equation 30 simplifies to

$$d\Delta N/dt \simeq P. \tag{32}$$

This has solution

$$\Delta N(t) = Pt + \Delta N_T, \tag{33}$$

where we have defined

$$\Delta N(t=0) = \Delta N_T \equiv \Delta N_{\text{THRESHOLD}}$$

Substituting equation 33 into 26

$$dU_M/dt = \sigma_M (c/L) U_M (Pt + \Delta N_T) - (c/2QL) U_M \qquad (34)$$

Now, at threshold $dU_N/dt = 0$, and using 26, equation 34 reduces to

$$dU_N/dt = \sigma_M (c/L) U_M \, Pt \qquad (35)$$

which has solution

$$U_M = U_{M_o} \exp (\sigma_M c P t^2/2L) \qquad (36)$$

where U_{M_o} is the total number of photons per unit area in the cavity when the inversion reaches the threshold value.

This solution is valid for $P \gg b\sigma_M (c/L) U_M \Delta N$. However, it may be used to estimate the inertial delay.

After the inertial delay the rate of stimulated emission has become equal to the pump rate such that equation 30 becomes

$$P = b \, \sigma_M (c/L) U_M \Delta N(\tau) \qquad (37)$$

Using equations 33 and 36 in 37

$$P = b \, \sigma_M (c/L) U_{M_o} \exp \left(\sigma_M \frac{cP}{2L} \tau^2\right) \quad (P\tau + \Delta N_T) \qquad (38)$$

from which we find

$$\tau^2 = \frac{2L}{\sigma_M c P} \ln \left\{ \frac{LP}{\sigma_M c U_{M_o} (P\tau + \Delta N_T)} \right\} \qquad (39)$$

Using equation 33 we may now write down an expression for the ratio of the maximum stored energy to the threshold inversion

$$\frac{\Delta N(\tau)}{\Delta N_T} = 1 + \frac{P\tau}{\Delta N_T}$$

$$= 1 + \frac{P}{\Delta N_T}\left\{\frac{2L}{\sigma_M cP} \ln\left[\frac{LP}{\sigma_M c U_{M_o} (P\tau + \Delta N_T)}\right]\right\}^{\frac{1}{2}} \tag{40}$$

Using equation 20, this becomes

$$\frac{\Delta N(\tau)}{\Delta N_T} = 1 + 2PQ\sigma_n\left\{\frac{2L}{\sigma_M cP} \ln\left[\frac{LP}{\sigma_M c U_{M_o}(P + 1/2Q\sigma_M)}\right]\right\}^{\frac{1}{2}} \tag{41}$$

The fundamental difference between an oscillator and an amplifier stage is characterized by the quality factor Q of the resonant cavity. Typical values for an oscillator and an amplifier are 0.83 and 0.07 respectively (5), and hence from equation 41 we expect the $\Delta N(\tau)/\Delta N_T$ ratio for the amplifier to be at least one order of magnitude less than for the oscillator and therefore the phenomenon of inertial delay cannot be used to advantage in an amplifier stage.

CHAPTER IV SECTION 3

GAIN

The laser pulse may be described in terms of the density of photons

$$q\ x,t)\ cm^{-3}.$$

This photon density is changed by stimulated and spontaneous emission and stimulated absorption. Since the lifetime for the excited state is 170 msec. (9) , the spontaneous emission process may be ignored and the photon density in an elementary volume which sweeps through the amplifier with velocity c will satisfy

$$dq/dt = \partial q/\partial t + c\ \partial q/\partial x = c\ \sigma_E\ q(t)\ n(t) \qquad (42)$$

where c is the velocity of light, n is the total inversion and σ_E is the effective cross-section defined by equation (12).

We consider the case where the inversion is changed only by stimulated radiative processes. That is, the pump pulse is considered to have terminated and both chemical deactivation and spontaneous emission are ignored.

Then

$$\begin{aligned} dn/dt &= dn_1/dt - (g_1/g_2)\,dn_2/dt = -dq/dt - (g_1/g_2)\,dq/dt \\ &= -\ (1 + g_1/g_2)\ dq/dt \\ &= -\ b\ c\ q\ \sigma_E\ n \qquad (43) \end{aligned}$$

where n_i is the population of the i-th energy level, g_i is the degeneracy of the level and

$$b \equiv (1 + g_1/g_2) \tag{44}$$

That is

$$dn/dt = -bcq\sigma_E n \tag{45}$$

Substituting this into equation 42 we find

$$\partial q/\partial t + c\,\partial q/\partial x = -\,1/b\ dn/dt \tag{46}$$

This may be integrated with respect to t, $0 \leq t \leq t_f$

$$q\Big|_0^{t_f} + d/dx \int_0^{t_f} cq(x,t)dt = \left(-1/b\right) n\Big|_0^{t_f} \tag{47}$$

We recognize cq = flux of photons and thus identify

$$\int_0^{t_f} cq(x,t)dt = \frac{\text{Total number of photons}}{\text{Unit area}} \equiv E(x) \tag{48}$$

Then (47) becomes

$$q(x,t)\Big|_0^{t_f} + d/dx\ E(x) = -1/b\ n(x,t)\Big|_0^{t_f} \tag{49}$$

We choose initial conditions and t_f such that

$$q(x,0) = q(x,t_f) = o, \quad 0 \leq x \leq L$$

as shown in figure 14.

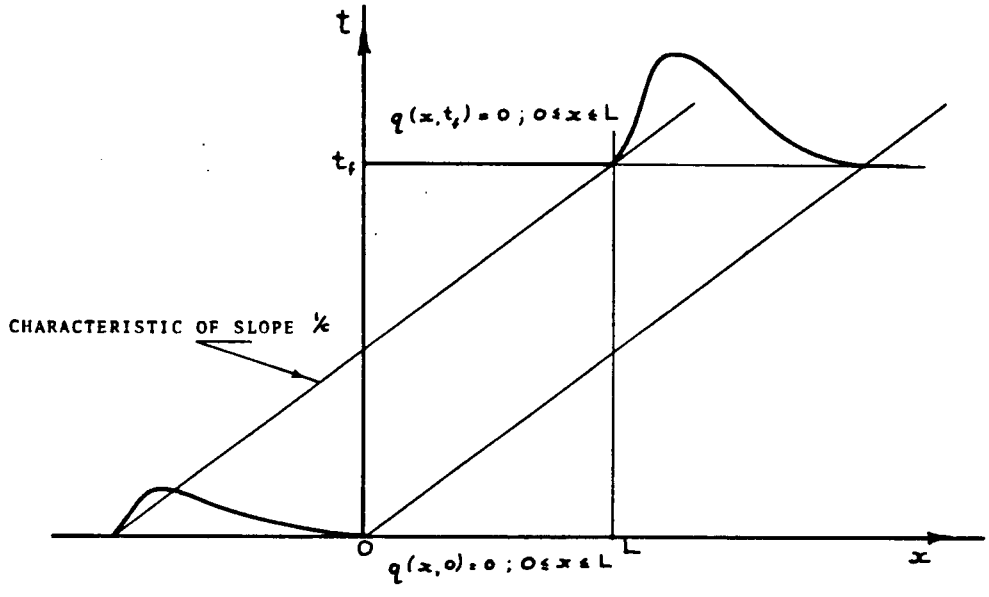

Fig. 14. The initial conditions and domain of integration of the differential equation characterizing the amplification of a laser pulse.

Then 49 becomes

$$d/dx\ E(x) = -1/b\ n(x,t) \Big|_{0}^{t_f}, \qquad 0 \leq x \leq L \qquad (50)$$

Rearranging equation 43 and integrating with respect to t

$$\int_{n(x,0)}^{n(x,t_f)} dn/n = \sigma_E b \int_{0}^{t_f} cq\ dt \equiv -\sigma_E bE(x) \qquad (51)$$

which has solution

$$n(x,t_f) = n(x,0)\ \exp.\ -\sigma_E bE(x) \qquad (52)$$

Using this in equation 50 we have

$$d/dx\ E(x) = -(1/b)n(x,0)\left\{\exp.\left[-\sigma_E bE(x)\right] -1\right\}$$
$$;\ 0 \leq x \leq L \qquad (53)$$

Finally, we integrate with respect to x, $0 \leq x \leq L$, and divide by E(0) such that

$$V \equiv \frac{E(L)}{E(x)} = \frac{1}{b\sigma_E E(0)} \ln\left\{1 + \left(e^{b\sigma_E E(0)} - 1\right) e^{\sigma_E n(t=0)L}\right\} \qquad (54)$$

<u>Small Signal Regime</u> $\qquad V_s = \lim_{E(0) \to 0} V$

In this regime the incident energy per unit area is small such that the inversion is not significantly depleted by stimulated emission.

For small $b\sigma_E E(0)$ we may expand the exponential $e^{b\sigma_E E(0)}$ and discard terms $0(b\sigma_E E)^2$.

Then

$$(e^{b\sigma_E E(0)} - 1)e^{\sigma_E n(0)L} \longrightarrow b\sigma_E E(0)e^{\sigma_E nL} \qquad (55)$$

Similarly, for $b\sigma_E E(0)e^{\sigma_E n(0)L}$ the logarithm may be expanded according to

$$\ln(1 + x) = x - x^2 + x^3 \ldots\ldots\ldots$$

and again terms $0(x^2)$ are discarded.

Equation (54) then becomes

$$V_s \simeq 1/bo_E E(0) \; (b\sigma_E \; E(0) e^{\sigma_M n(0)L})$$
$$= e^{\sigma_E n(t=0)L} \qquad (56)$$

Using equation 20 and 56 we find that the maximum small signal gain V_{SM} is completely defined by the quality factor Q of the cavity

$$V_{SM} = e^{1/2Q} \qquad (57)$$

Typical values of $V_{SM} = 10^3$ are achieved for amplifiers by careful mechanical design and the avoidance of reflectory surfaces (5).

Large Signal Regime

The incident signal is large such that the inversion is totally depleted.

For E(0) large, equation 54 reduces to

$$V_L \simeq \left(1/b\sigma_E E(0)\right) \ln \; \exp. \; b\sigma_E E(0) \; \exp. \; \sigma_E n(0)L$$

$$= 1 + \frac{n(t=0)}{bE(0)} \qquad (58)$$

V_S is typically two orders of magnitude greater than V_L, resulting in a change in the temporal profile of an energy pulse as it passes through the amplifier. (See Chapter 4.8)

CHAPTER IV SECTION 5

EXTRACTION RATIO

The extraction ratio of an amplifier is defined as

$$\equiv \frac{E_{OUT} - E_o}{E_{STORED}} \tag{59}$$

E_{OUT} (E_o) is the total output (input) energy per unit area and E_{STORED} is the total energy per unit area stored in the laser medium.

The maximum extraction ratio occurs when the incident pulse has energy density in the large signal regime throughout the amplifier. This yields an extraction ratio of 0.66 due to the degeneracy of the energy levels.

CHAPTER IV SECTION 6

SATURATION ENERGY DENSITY

Choosing the condition $e^{b\sigma_E E(0)}$ 5 to define the large signal regime, the incident energy density to achieve the maximum extraction ratio E_S, may be evaluated.

$$E_o = \frac{\ln 5}{b\sigma_E} \tag{60}$$

CHAPTER IV SECTION 7

BEAM QUALITY

In order to preserve the beam profile and minimize its divergence it is important to generate an homogeneous inversion.

An empirical formula relating the laser tube diameter and pressure of the active medium has been determined by K. Hohla et al (21)

$$P = 170 \times D^{-1} \text{ Torr} \qquad (61)$$

where P is the pressure of the active gas and D is the diameter of the laser tube in centimeters.

This homogeneous inversion can be disturbed by a shock wave generated by the vaporization by the pump light, of deposits condensed on the tube wall (18, 22). Pumping must be terminated and the stored energy released before the shock wave has propogated a significant distance, thereby destroying the homogeneity.

An estimate of the shock velocity of 3×10^4 cm/sec or 0.3 mm/per sec (6) may be used to evaluate the loss of active volume as a function of ellapsed time after the initiation of the pump pulse.

The first and second amplifiers of the IPP, Garching, system use a high capacitor changing voltage and consequently a short duration pumping pulse (17). During the

resulting 6 μs pulse the shock wave propogates only 1,8 mm and the major portion of the activated medium is undisturbed. However, the lower charging voltage used at the Sandia Laboratories (6) results in a 20 μs current pulse and therefore a significant loss in the unperturbed active region. (See Chapter 4.11)

Experiments conducted at the Sandia Laboratories demonstrated that the shock wave is driven by heat absorbed in carbon deposited on the tube surface. This carbon results from the photolysis of iodine compounds at wavelengths less than 200 nm and can therefore be avoided by filtering out these wavelength components from the pump light. It was found that using laser tubes made from Germisil, a Titanium doped quartz which is opaque at wavelengths less than 200 nm not only eliminated the shock wave but also the brown-black surface deposits which after 20 shots absorb approximately 20% of the UV pumplight (6).

CHAPTER IV SECTION 8

PULSE SHAPE MODIFICATION

As an energy pulse passes through the amplifier, two processes operate simultaneously to modify its temporal profile.

1. The finite bandwidth of the amplifier has the effect of attenuating the higher order Fourier components and therefore broadening the pulse.

2. A pulse passing through a section of the amplifier depletes the inversion and therefore the initial part of the pulse is amplified more than the later part. Thus the pulse profile becomes skewed and the half width is reduced.

For a rigorous theoretical treatment of this phenomenon the reader is referred to a paper by J. N. Olsen (23).

CHAPTER IV SECTION 9

EFFICIENCY

The efficiency of an amplifier is defined as the ratio of the energy extracted from the active medium by the laser pulse, to the energy stored in the capacitor. It has a maximum value of approximately 1% limited primarily by the difference between the broad spectrum of light produced by the Xenon flash tubes and the narrow absorption line of CF_3I at 2660A^{o}. Pressure broadening this line and a careful choice of Xenon gas fill pressure in the flash tubes to maximize the light output in this spectral region, improves the efficiency.

Imperfect optical coupling between the flash tubes and the active medium also reduces the system efficiency. The

flash tubes must be positioned such that the angle subtended between the arc and the active volume is maximized. Light which is not emitted into this angle must suffer a reflection at the surrounding mirror before entering the active medium.

Research is in progress to define the optimum choice of material for these mirrors since much of the light undergoes multiple reflections (6). Aluminum foil is being used at present in the laser at the University of British Columbia.

Pumping the laser medium above the threshold for parasitic oscillation, chemical deactivation during long pumping pulses and optical coupling losses also results in a significant reduction in the system efficiency.

Typical efficiencies of 0.1 and 0.3% for preamplifier and final amplifier stages respectively are being measured (17, 24).

CHAPTER IV SECTION 10
THE BUFFER GAS PRESSURE

Typical buffer gasses are CO_2 and Argon. Increasing the pressure of the buffer gas in the mix has the following advantages.

1. The bandwidth of the amplifier is increased (page 14).

2. The maximum stored energy is increased (page 28).

3. The temperature rise of the gas mix during photolysis is reduced, thereby keeping the rate coefficients for the chemical deactivation process to a minimum (page 28).

4. The coupling efficiency of the pump pulse light to the active medium is improved by pressure broadening.

There are two disadvantages:

1. The extraction ratio is reduced (page 47).

2. Chemical deactivation by the buffer gas is increased.

For subnanosecond laser pulses the buffer gas pressure is defined by the bandwidth necessary to ensure an acceptable amount of pulse broadening (page 15).

CHAPTER IV SECTION 11
THE FLASH TUBE CIRCUIT

The design of the flash tube circuit system may be separated into two distinct forms which we call the high voltage and low voltage schemes.

In the high voltage scheme a high intensity short duration pumping pulse (typically 6 μs.) is produced, whereas the

low voltage system results in a much longer (typically 20 μ s.) and less intense pulse.

We examine the design compromises inherent in each scheme.

The High Voltage Scheme

Advantages

1. The effect of chemical deactivation is small if the energy is stored and released within a time short compared with the half life of I* due to these processes.

2. A shock wave will only propagate a small distance inwards from the wall of the laser tube disturbing the optical homogeneity of the medium.

3. If the pumping pulse is short enough to deliver a significant amount of energy during the inertial delay of the system, then the stored energy density can exceed the threshold for parasitic oscillation.

Disadvantages

1. A higher voltage, and consequently more expensive, power supply is required to charge the capacitor.

2. The electric insulation must be designed for the high working voltage.

3. More flash tubes are required to deliver the same energy.

The Low Voltage Scheme

Advantages

1. A less expensive lower voltage power supply is required.

2. The electric insulation suitable for the lower working voltage is sufficient.

3. More energy can be delivered by fewer flash tubes than in the high voltage scheme.

Disadvantages

1. Significant chemical deactivation occurs during the long pump pulse.

2. A shock wave will disturb a large volume of active medium.

3. Very little energy is delivered during the inertial delay of the system.

CHAPTER V THE SYSTEM DESIGN PROCESS

Having derived the relationship between the system design, operating conditions and performance, the design process may proceed. This involves finding a route through the Polya-Fuller map until all of the variables are defined.

CHAPTER V SECTION 1
THE GIVEN VARIABLES

The first stage in the design process is to list the system variables which are given (see Figure 15).

1. Incident Energy e_o. The incident energy is expected to be approximately 100 mJ in a pulse of duration 1 ns. (24)

2. Beam Quality: The inversion density must be uniform and no optical inhomogeneities due to turbulance should be present in the active volume of the laser medium.

3. Efficiency: Minimum value 0.1%.

4. Lifetime: The lifetime of the flash tubes should exceed 1500 shots (5).

5. Q for Parasitic Modes: Typically this has a value which leads, via equation 52, to a maximum small signal gain of 10^3
i.e. $V_{SM} = 10^3$.

6. Laser Tube Diameter: 2.5 cms. Defined by the divergence of the beam and separation required for optical isolation.

7. Reflection Material: Aluminum foil.

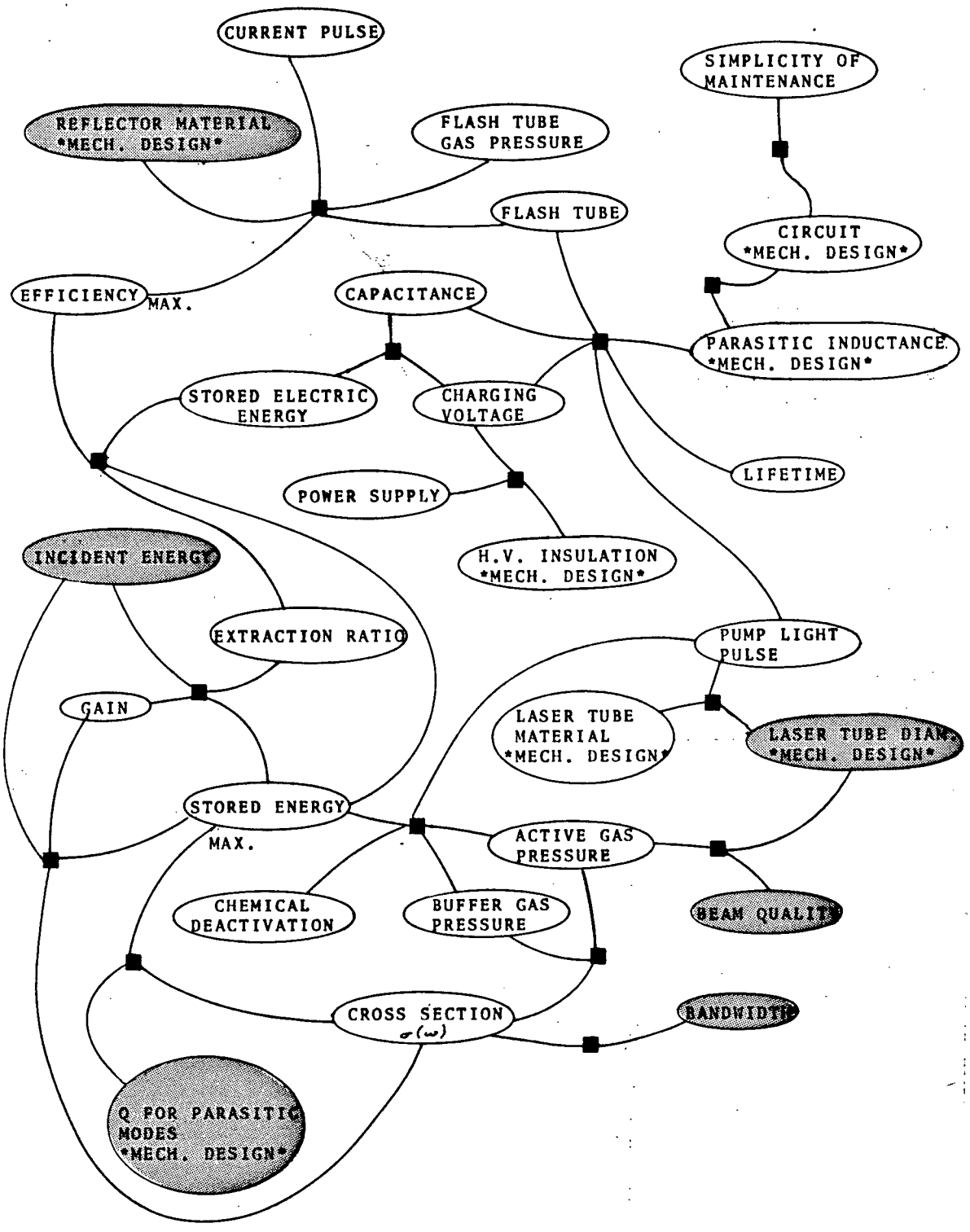

Fig. 15. System design diagram indicating the given variables.

CHAPTER V SECTION 2

THE GAS PRESSURES

Refer to Figure 16.

Having chosen the laser tube diameter to be 2.5 cms., the pressure of the active gas required to produce an homogeneous inversion is defined by equation (61).

i.e. $P = \frac{170}{2.5} \simeq 70$ Torr

The minimum buffer gas pressure to provide the required bandwidth is 400 Torr CO_2 (Chapter 4.2). Increasing this pressure raises the threshold for parasitic oscillations and consequently the maximum stored energy. It is important to pump the medium to this energy density such that the maximum small signal gain is attained. This ensures that the laser pulse is amplified to the local saturation energy density within a short distance and hence a good extraction ratio is achieved.

It turns out to be difficult to arrange a sufficient number of flash tubes to achieve a large stored energy around the small diameter laser tubes. Hence, for a short duration laser pulse, the buffer gas pressure is completely defined by the bandwidth requirement.

The effective cross-section for a gas mix of 400 Torr CO_2 and 70 Torr CF_3I is found to be

$$\sigma_E \simeq 3 \times 10^{-19} \text{ cms.}^2 \qquad (7)$$

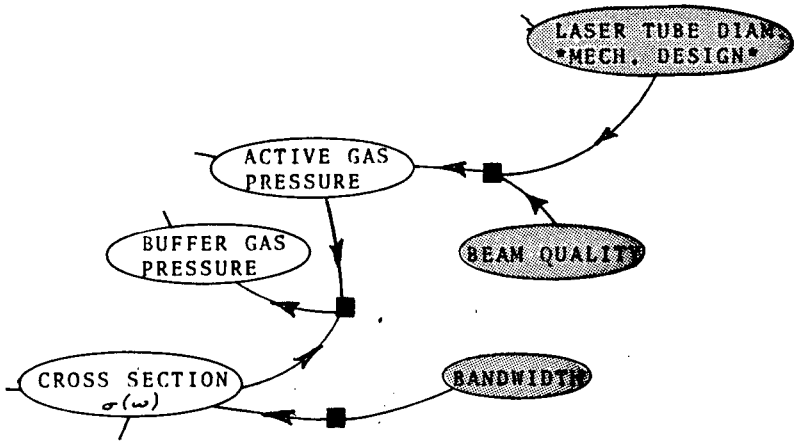

Fig. 16. The Section of the System Design Diagram which is used to define the gas pressures.

CHAPTER V SECTION 3

THE STORED ENERGY, GAIN AND EXTRACTION RATIO

Refer to Figure 17.

Using a typical value maximum small signal gain (Chapter 4, Section 3) the maximum stored energy is calculated using equation (56).

$$V_{SM} = 10^3 = e^{\sigma_E \Delta N_T}$$

$$\Rightarrow \Delta N_T = 2.3 \times 10^{19} \text{ photons-cms}^{-2}$$

$$\simeq 3.5 \text{ J cms}^{-2}$$

Using equation 54 the gain may bow be evaluated.

$$V = \frac{1}{b\sigma_E E_0} \ln \left\{ 1 + (e^{b\sigma_E E_0} - 1)\, e^{\sigma_E \Delta N_T} \right\}$$

We first evaluate the incident energy density in units of photons cms^{-2}

$$E_0 = \frac{\text{Incident Energy (Joules)} \times (\text{eV - Joule}^{-1})}{\text{Cross-sectional Area of Medium} \times (\text{eV - photon}^{-1})}$$

$$\Rightarrow E_0 \simeq 1.3 \times 10^{17} \text{photons - cm}^{-2}$$

Substituting into equation 54 we find

$$\underline{V \simeq 62}$$

The extraction ratio may now be found using equation 59

$$\eta = \frac{V \times E_0 - E_0}{(E_{STORED} \equiv \Delta N_T)} - 0.34$$

$$\underline{\eta = 0.34}$$

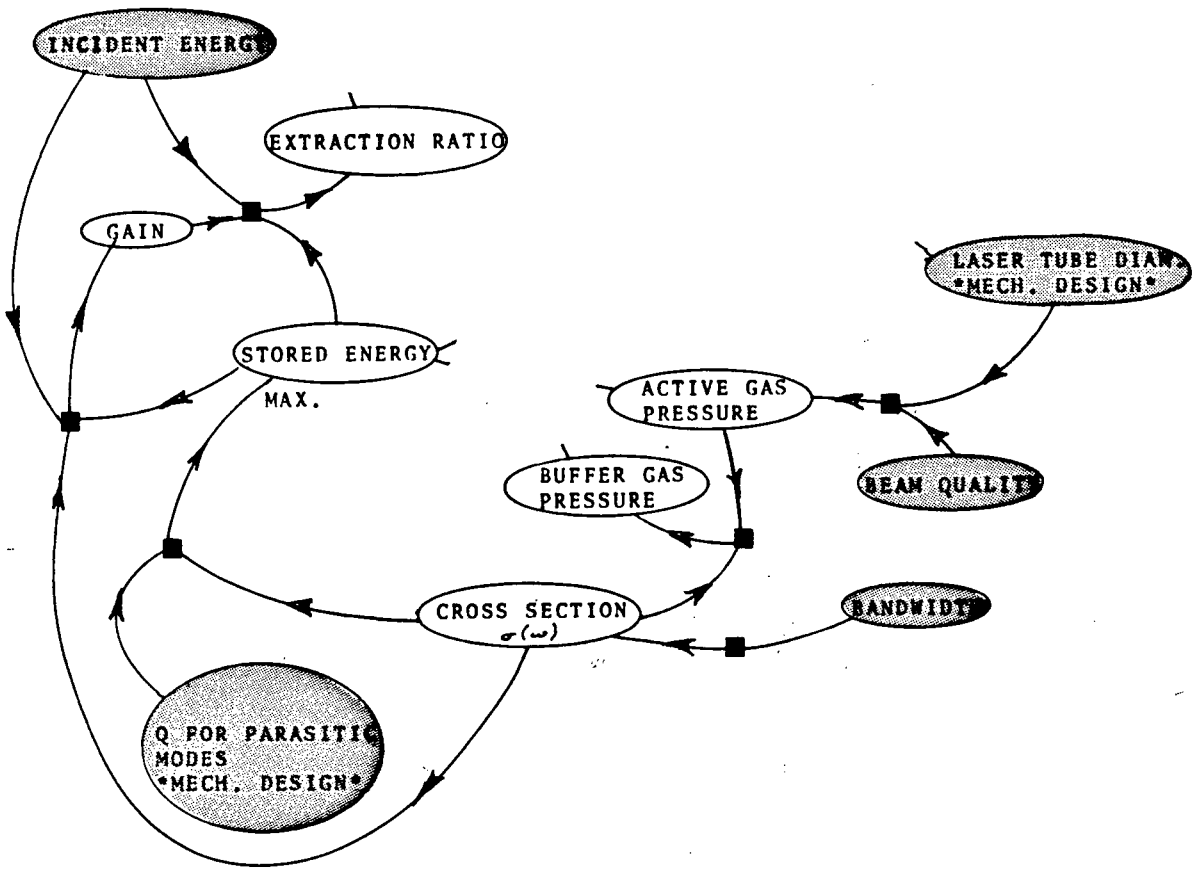

Fig. 17. The section of the system design diagram used to define the stored energy, gain and extraction ratio.

CHAPTER V SECTION 4

THE STORED ELECTRIC ENERGY

Figure 18 shows the system design for the stored electrical energy.

For a preamplifier stage the efficiency is typically 0.1% (Chapter 4.9).

The energy extracted from the laser medium, evaluated from the extraction ratio and the stored energy, together with the value for the efficiency may be used to estimate the total energy to be stored in the capacitor.

$$\text{Stored Electric Energy} \simeq \eta \times \text{Stored Energy} \times \left(\frac{0.1}{100}\right)^{-1}$$
$$\simeq 6 \text{ KJ}$$

This value, being derived from an estimate of the efficiency, is only approximate. The Q for parasitic modes may also be somewhat less than the value chosen, thereby allowing for a higher stored energy density. Thus the system response to an increase in the stored energy in the capacitor should be studied experimentally. The gain would be expected to increase with stored electric energy until the threshold for parasitic modes is reached.

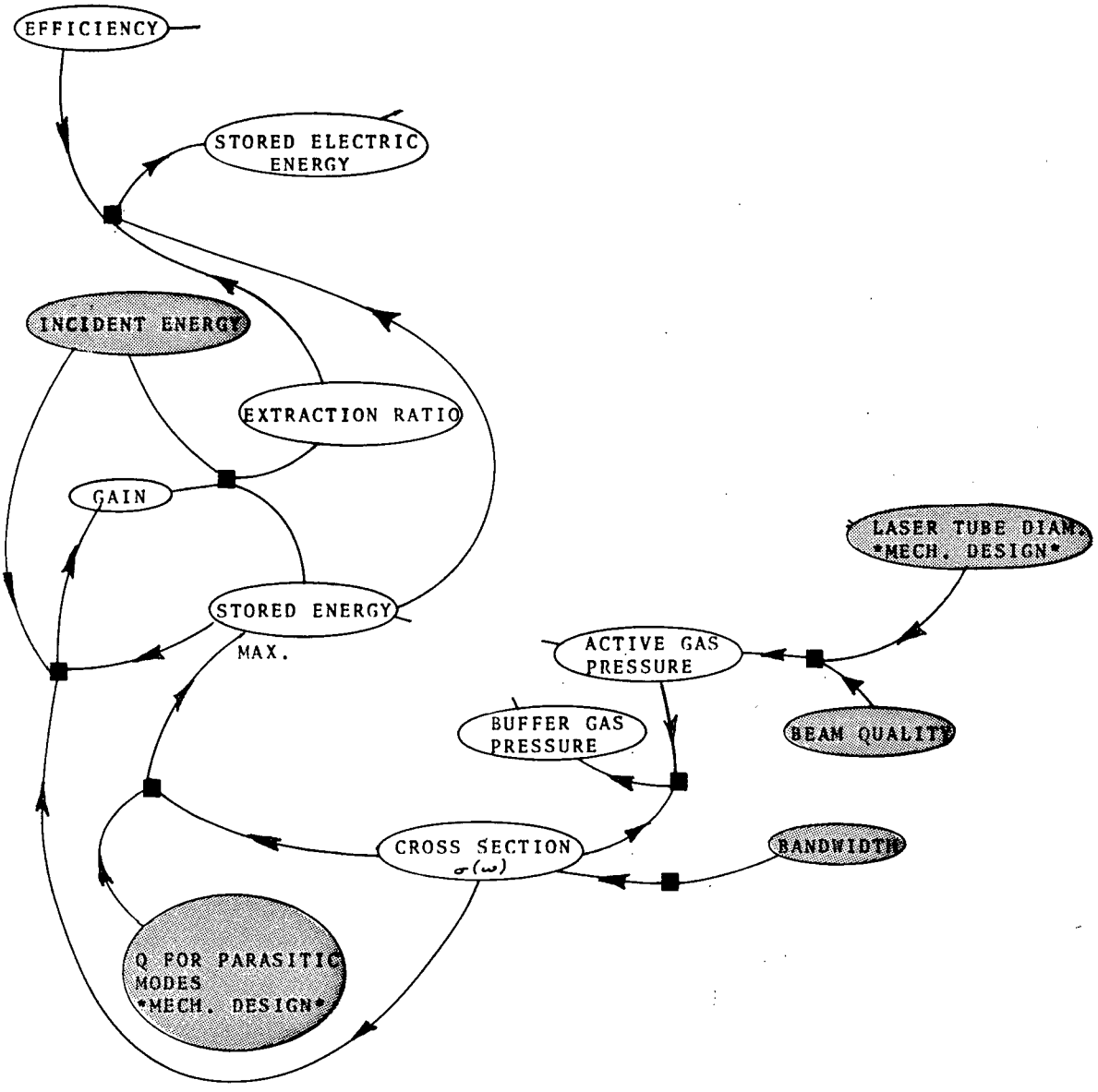

Fig. 18. The section of the system design diagram used to define the stored electric energy.

CHAPTER V SECTION 5

THE ELECTRICAL SYSTEM AND PUMP LIGHT PULSE

Figure 19 shows the relevant section of the system design diagram.

In order to proceed with the design of the remainder of the system, a choice between the high and low voltage schemes for the flash tube circuit, as discussed in Chapter 4.11, must be made. Before the work of R. E. Palmer et al (6) showing that shock waves no longer occur when Germisil laser tubes are used, the choice was not obvious. However, the low voltage system is clearly superior if this problem is eliminated.

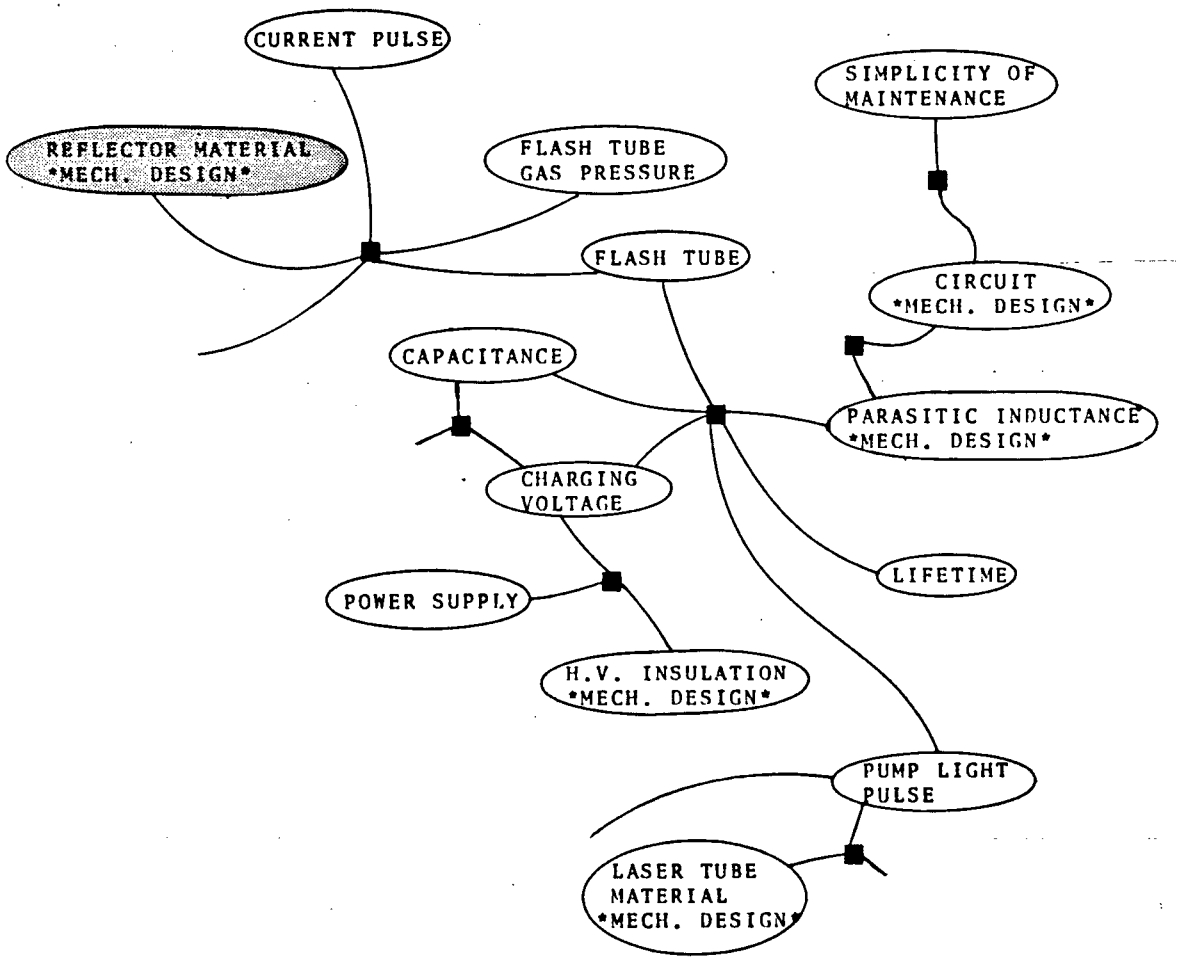

Fig. 19. The section of the System Design Diagram containing the remaining undefined variables.

The Low Voltage Scheme

Xenon flash tubes with an arc length of 61 cms., and an explosion energy of 2500 Joules were selected. The recommended energy and current are 2000 Joules and 6 KA respectively.

The flash tube circuit consists of a capacitor, the parasitic impedance of the circuit, and the flash tube connected in series. It is important to choose the mechanical design of the circuit to minimize the parasitic impedance and thereby produce a short critically damped current pulse.

The voltage-current characteristic of the flash tubes has the form (9).

$$V = K_o I^{\frac{1}{2}} \tag{62}$$

where K_o is given by

$$K_o = k \frac{l}{d} \tag{63}$$

and l is the length of the lamp in cms., d is the bore diameter in cms., and k is a function of the type of gas and its pressure (typically 1.2); (9)).

We find $K_o \simeq 104 \Omega A^{\frac{1}{2}}$ for this flash tube.

Solution to the non-linear differential equation for the series circuit are presented in a paper by Holzrichter and Schawlow (25).

The duration of the current pulse should be tailored to deliver the energy in as short a time as possible, to minimize the losses due to chemical deactivation, without exceeding the maximum recommended operating current. An upper bound of 20μs for the pulse duration is suggested by an examination of the chemical deactivation rates.

In order to derive an approximate relation between the maximum current, the stored energy and the pulse duration, the critically damped current pulse may be trated as a sine function ($0 \leq t \leq \pi$).

Using the model we find

$$I_M \simeq \left\{ \frac{1.8E}{K_o} \right\}^{2/3} \quad A \qquad (64)$$

where

I_M = maximum current in amps.
E = stored electric energy in Joules
= pulse duration in seconds

If eight flash tubes are used then 6K Joules of energy delivered in a 20μs pulse yields a maximum current of 7.5 KA in each flash tube.

This exceeds the maximum operating current and therefore more flash tubes must be used or the total energy or the tube lifetime sacrificed.

We choose to use eight flash tubes for the following reasons:

1. Two are required to illuminate the full length of the amplifier and thus the total number must be raised to ten, thereby increasing the cost and the complexity of the mechanical design considerably.

2. The function of a preamplifier is to raise the energy of the beam to the saturation density of the final amplifier. This may be possible with a reduced stored energy density.

3. The stored energy required is based on an estimate of the system efficiency and may therefore be less than the calculated value.

4. The operating energy is well below the maximum suggested by the manufacturer, and the design lifetime of 1500 shots may be attainable even with a maximum current 25% above the recommended value.

Using a Rogowski coil we measured the current pulses with both 10 and 20μf of capacitance in the circuit. They were critically damped and had a duration of approximately 9 and 12μs respectively.

The pulse duration is proportional to $\sqrt{LC}$ (9) and inserting the experimentally measured values into this

relation we deduce that the parasitic impedance is not changed appreciably by adding capacitors. Thus we calculate that 40 and 50μf will result in pulses of approximately 18 and 21μs duration respectively.

The following table lists the calculated values of the pulse duration, stored energy and maximum current for a 40 and a 50μf capacitor bank.

		STORED ENERGY = 6KJ		MAX. CURRENT = 6KA	
CAPACITANCE μf	PULSE DURATION μs	I_M KA	CHARGING VOLTAGE	STORED ENERGY	CHARGING VOLTAGE
40	18	8·1	17 KV	3·9KJ	14 KV
50	21	7·3	15 KV	4·5KJ	13 KV

Table 1. Current pulse characteristics for capacitor bank.

A capacitance of 40μf and a charging voltage of 14 KV is chosen to deliver 3.9KJ within a pulse of duration 18μs.

Having specified the current pulse, the optimum Xenon gas fill for the flash tubes may now be found from the manufacturer's specifications.

Reducing the stored electric energy from the optimum value of 6KJ to 3.9 KJ will lower the inversion and consequently the system gain. Assuming the inversion is reduced by one third to 2.3 J/cm.^{2} we find that the system gain and extraction ratio are reduced to

$$V \simeq 33 , \quad \eta \simeq 0.28$$

The buffer gas pressure could be reduced to improve the extraction ratio at the expense of the amplifier bandwidth if this design compromise was more acceptable.

Summary

"Germisil" laser tubes must be used to contain the active gas mix of 70 Torr CF_3I and 400 Torr CO_2.

Eight Xenon flash tubes connected in parallel and driven by a 40μf capacitor bank charged to 14 KV will result in a gain of 33 and an extraction ratio of 0.28.

If necessary, the charging voltage may be increased to 17 KV to overdrive the flash tubes, after the effect on the lifetime has been measured experimentally.

CHAPTER V SECTION 6
MECHANICAL DESIGN

Summary of Mechanical Design Requirements

1. Simple routine replacement of defective Xenon flash tubes.

2. Laser tubes to be easily removable for cleaning or replacement.

3. Minimum parasitic inductance of the electric circuit.

4. Flash tubes located as close as possible to the laser tube.

5. Inner surface of laser tube to be etched to improve homogeneity of inversion.

6. Aluminum foil used as reflector.

7. Germisil laser tubes to eliminate shock waves and absorption by wall deposits.

8. Electric insulation suitable for a working voltage up to 20 KV.

9. Vacuum system able to achive a pressure less than 10^{-2} Torr.

The Apparatus

The inversion is created within two identical cylindrical sub-assemblies 75 cms. long and 11.5 cms. in diameter each containing four Xenon flash tubes and a laser tube 85. cms. long. The laser tube is located on the subassembly axis by holes in two acrylic end plates. The tube ends, protruding from these sub-assemblies, are joined by a "Y" shaped O ring sealed coupling, the centre leg of which is connected via a cold trap to both mechanical and diffusion vacuum pumps.

Quartz windows at the Brewster angle are mounted in assemblies which are O-ring sealed to the outer ends of the laser tube. Evacuation of the tube draws these window assemblies firmly against the acrylic end plates.

The set of four flash tubes are clamped between two aluminum collars and aluminum foil is wrapped around the outside to act as the reflector. This unit is accurately located within the cylindrical sub-assembly by recesses in the acrylic end plates, which match the aluminum collars (see figure 20).

Simple removal of both the laser tubes and the flash tubes is therefore achieved. A laser tube may be pulled out after loosening the "T" shaped O ring coupling. The unit, consisting of four flash tubes and reflector, slides out of the assembly after removing an acrylic end plate.

Each sub-assembly also contains a cylindrical copper return conductor which is held in position by acrylic rings. Electrical connection to the flash tubes is made via holes drilled through the acrylic end plates and into the aluminum collars. Two coaxial cables, one from each set of four flash tubes, are brought in parallel to the spark gap. This coaxial spark gap is located directly above the capacitor bank which is positioned adjacent to the amplifier in order to minimize the parasitic inductance of the circuit.

CF_3I was supplied in 100 gm. cylinders by P.C.R. Research Chemicals, Florida, U.S.A., and research grade CO_2(99.995%) supplied by Matheson Gas Products was used as the buffer.

A small mixing chamber (4.5 cms. diameter x 10 cms. long) containing a steel rotor, coupled through the brass wall to a rotating magnet, is provided to reduce the time required for these gasses to mix.

Narrow bore copper tubing is used throughout to transport the gasses.

Silicon controlled rectifier (SCR) units are used to trigger the discharge of the capacitor banks of the oscillator and amplifier stages. These SCR units are themselves triggered via adjustable electronic delays from a pulse generator. The delay between the pulse from the generator and the triggering of each SCR unit is used to set the arrival time of the laser pulse at the amplifier to coincide with the maximum stored energy.

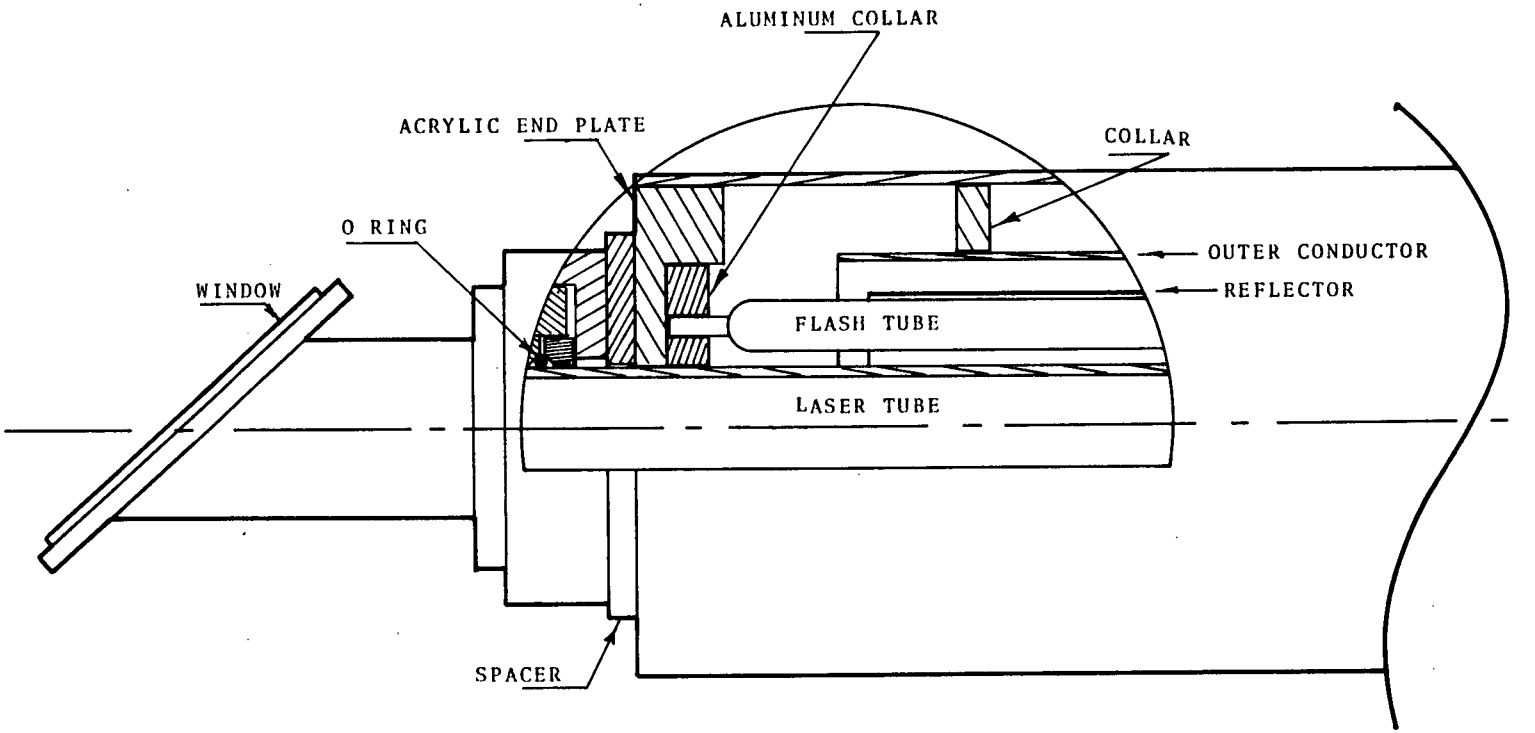

Fig. 20. Details of a cylindrical sub-assembly and an O ring sealed window assembly.

CHAPTER VI DIAGNOSTICS

Current Pulse Profile and Timing

Rogowski coils are used to monitor both the oscillator and amplifier flash tube current pulses. The integrated pulses from these coils are displayed on a dual beam Tektronix 531 oscilloscope and recorded photographically each time the laser is fired. (See figure 21)

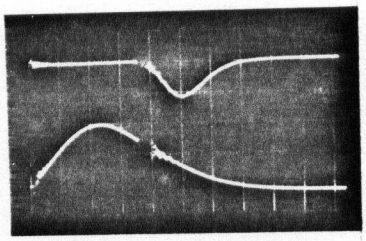

2μs/DIV.

Figure 21. Current Pulse Profiles. The current pulses driving the oscillator (upper) and the amplifier (lower) flash tubes are shown.

These photographs are used to measure the reproducibility of the pump light pulses and also the time of arrival of the laser pulse at the amplifier. Noise, generated by the SCR pulse, also appears on these photographs and therefore the spark gap timing jitter may be measured.

Amplifier Gain and Temporal Profile of the Laser Pulse

Two Indium antimonide photoconductive detectors (Mullard ARPIO) and a Tektronix type 554A oscilloscope are used to observe the incident and amplified laser pulse. The signals from the detectors are delayed in order that they do not coincide with the noise generated during the pump light pulse.

The "y" amplifiers of the oscilloscope are used in the A + B mode such that both signals can be displayed simultaneously by using a different delay in the cables from the two photoconductive detectors. (See figure 22)

5mV/DIV.

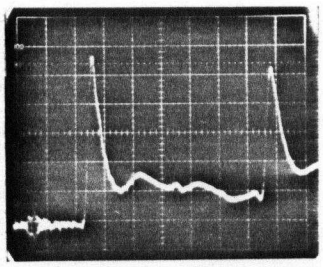

1μs/DIV.

Fig. 22. The incident and amplified laser pulses. The output from the two photoconductive detectors is shown, the first (second) being generated by the amplified (incident) laser pulse.

The detectors begin to saturate at an output of 50 mV and therefore an oscilloscope sensitivity of 5 mV per division is appropriate. The amplified laser pulse is attenuated using calibrated neutral density filters to maintain the signal level within the linear region.

This scheme clearly displays the modification of the pulse shape by the amplifier.

Beam Profile

Mechanical adjustments are provided to allow the measurement of the intensity profile of the beam. A micrometer screw on the mirrow mounts located as shown in Figure 5.5 provide for a vertical sweep of the beam across the photoconductive detector. Horizontal adjustments are achieved by changing the position of the screw slides on which the detectors are mounted.

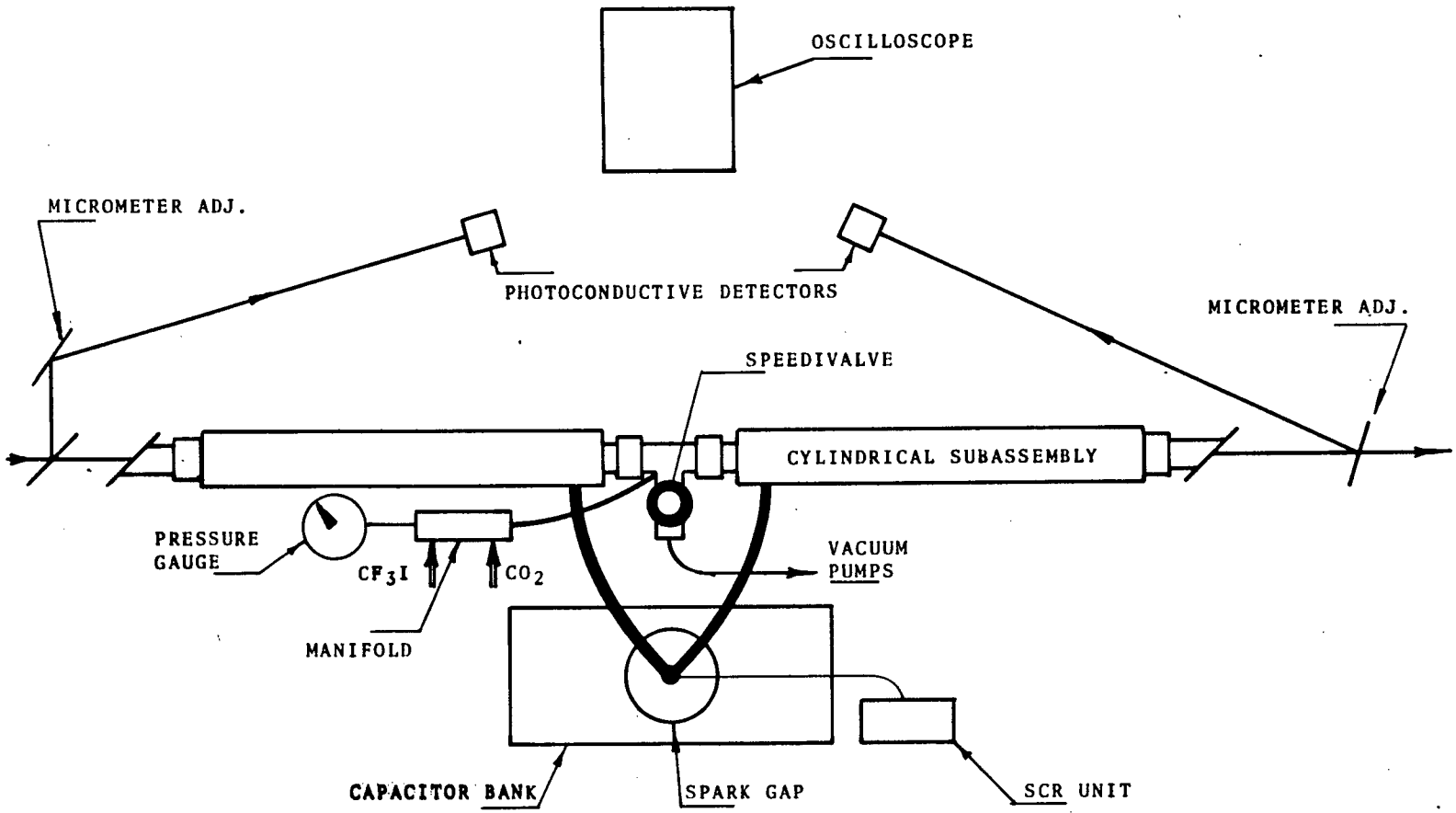

Fig. 23. Schematic diagram of the amplifier and associated diagnostics.

CHAPTER VII THE EXPERIMENT

The Vacuum System

Some difficulty was experienced in achieving the O ring vacuum seals to the laser tubes which were not round and had surface imperfections. After some experimentation it was found that thin brass collars, which would distort to the non-round cross-section and provide a smooth surface, could be glued to the tubes. The O rings were able to accomodate the non-circular cross-section.

A number of leaks were traced to blemishes on the O ring surfaces of the "Speedivalves" used in the system. Since these valves were cast from aluminum they are easily scratched and care must be taken to avoid damaging them on installation.

Residual paste flux, used when soldering the copper tubes to the speedivalve couplings was found to be very difficult to remove. These tubes were replaced by others on which acid flux was used. This is easily removed by rinsing in hot water and after this treatment outgassing is complete within 24 hours.

The oil rotary and diffusion pumps evacuated the completed system to 0.6×10^{-3} Torr and at this pressure the leak rate was found to be 0.1×10^{-3} Torr per minute.

The Capacitor, Spark Gap, Flash Tube Circuit

The current pulse in the circuit was found to be critically damped and the addition of more capacitors to the bank did not increase the inductance of the circuit appreciably. (Chapter 4.11)

In order to minimize the timing jitter of the current pulse it was necessary to adjust the separation of the spark gap electrodes so that the discharge would occur spontaneously at approximately 200 volts above the working voltage. Rapid changes in the relative humidity of the atmosphere made it difficult to maintain this current gap setting.

With careful adjustment of the spark gap no difference in the timing or profile of the current pulse would be

observed from pulse to pulse. However, after approximately 250 shots a misfire occasionally occurred. A glass tube insulator is included in the spark gap so that the diameter of the outer conductor, and consequently the inductance of the switch, may be reduced. After replacing this tube the misfire did not occur, suggesting that metal deposits formed on the wall of the tube had provided an alternate path to ground for the discharge.

Measurement of the Profile of the Incident and Amplified Laser Pulse

The use of delays to shift the signal away from the noise produced by the flash lamp circuits was only partially successful. A burst of noise lasting approximately 200 ps. with periodicity $2\frac{1}{2}\mu s$, persisted well into the interval when the laser pulse was displayed. This noise is particularly troublesome as it completely obscures the leading edge of the laser pulse.

Experiments were conducted to minimize the capacitive and inductive coupling of the diagnostic circuit from the flash tube circuit. A different ground circuit was used for these two systems and care was taken to shorten cables and eliminate loops.

The most obvious improvement was made by repositioning the photoconductive detectors further away from the amplifier assembly, on an electrically non-conducting table.

However, the periodic noise was still troublesome and additional changes were required.

The SCR unit discharges a 1μf capacitor into a transformer, the secondary winding of which is connected to the spark gap trigger electrodes. This secondary unit was found to be resonating (see Figure 23) and each time the current passes through zero and the arc was re-established, the noise burst appeared.

The period of this resonance was found to be very sensitive to the stray capacitance in the circuit. Even the capacitance of the cable to the oscilloscope, used to observe the current flow, reduced the period of the oscillation to 0.6μs. (See Figure 24) Locating the SCR unit only 25 cms. away from the spark gap, and keeping the two wires connecting the secondary of the transformer to the trigger electrodes physically separate, critical damping was achieved and the periodic noise eliminated.

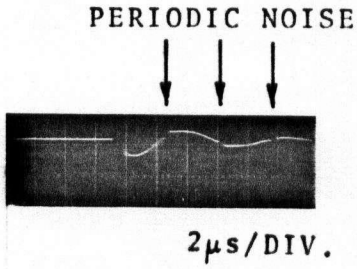

Fig. 24. The current flow in the secondary winding of the SCR trigger transformer. Noise is seen to occur each time the current passes through zero.

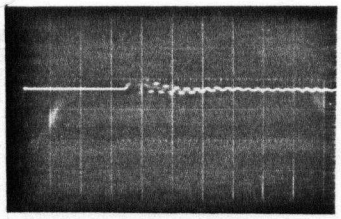

2μs/DIV.

Fig. 25. The current flow in the secondary winding of the SCR trigger transformer is shown when a long cable to the oscillation is used.

Timing of Arrival of Incident Laser Pulse

A great deal of difficulty was experienced in achieving the required delay (6-12 μs) between the initiation of the discharge of the amplifier and oscillator capacitor banks. It was found that the electric noise, associated with the discharge of the amplifier capacitor bank, which reaches a maximum current of 48 KA, caused the oscillator SCR to fire.

Initially it was believed that the noise was coupled to the SCR unit via the grounding circuit and therefore the following improvements were made:

1. The optical bench was used as the single ground conductor, one end being connected with heavy copper braid to the laboratory buss bar.

2. The power supplies and capacitor banks were connected to the bench separately, using short cables.

3. Grounding of the power supplies through the A.C. line cables was eliminated.

4. All connections in the ground circuit were cleaned and tightened to minimize the contact resistance.

The timing problem persisted. However, having made these changes it was decided that impedance of the ground circuit, and hence the noise signal, had been minimized and that no further improvements would be made in this system. The next series of experiments were therefore aimed at improving the noise immunity of the delay and SCR units.

Measurement of the noise level at different locations in the circuit was impossible since the signal is so pervasive that it appears on the oscilloscope even when no input cable is connected.

The noise causing the timing problem was found to occur during the initiation of the arc in the spark gap and the SCR unit was found to be triggered even when removed some distance from the laser, indicating that the coupling was, in part, radiative. Shielding the spark gap made no noticeable difference and thus it was concluded that the flash tube circuit acts as an antenna for the radiation.

Improved shielding and wiring to the printed circuit board, and the addition of small decoupling capacitors in the SCR circuit to provide a low impedance to ground for the

high frequency noise eliminated the problem, unless a cable was connected to the trigger terminal. Having excluded the noise from the SCR shielded can, a monostable delay, carefully shielded, was installed within the unit so that for correct timing a trigger pulse would be required to arrive before the noise signal. The circuit used did not function as required, since the noise reset the monostable. However, by making the delay only one $1\mu s$ and utilizing the noise immunity of the input required to set the monostable, correct timing was achieved.

The following additional improvements were also made:

1. The trigger pulse for the oscillator delay unit was derived from the light output of the amplifier flash tubes via an optic fibre which is immune to electric noise.

2. Flash tube light and an optic fibre were also used to trigger both oscilloscopes, thereby eliminating an additional 15 feet of cable.

3. The trigger and noise signal appearing at the monostable input was clamped by a zener diode. Since the noise occurs as an oscillation about the d.c. level of the trigger pulse, this clamping at a low voltage will eliminate much of the noise signal.

Although this system is now functioning as required, some triggering difficulties may be encountered when the

final amplifier is operated. Changing the integrated circuit used in the SCR unit from a retriggerable to a latched monostable (e.g., Fairchild type 9203), will enable the circuit to be operated as proposed, providing a much improved noise immunity.

Preliminary Experiments with the Complete System

Preliminary experiments with the apparatus in the present stage of construction were performed in order to check the operation of the entire system, including the diagnostics, and identify possible difficulties which may be encountered in the future.

At present the apparatus has a 20μf capacitor bank, uses quartz laser tubes, and operates in the low voltage regime. In order to perform the experiments and avoid the difficulties associated with the shock waves inevitable with the device in its present form, a spatial filler was used to limit measurements to the undisturbed beam centre. Operating at low pressure, i.e., without any buffer gas, the laser pulse was passed through the amplifier at various times during the pump pulse (see Figure 26).

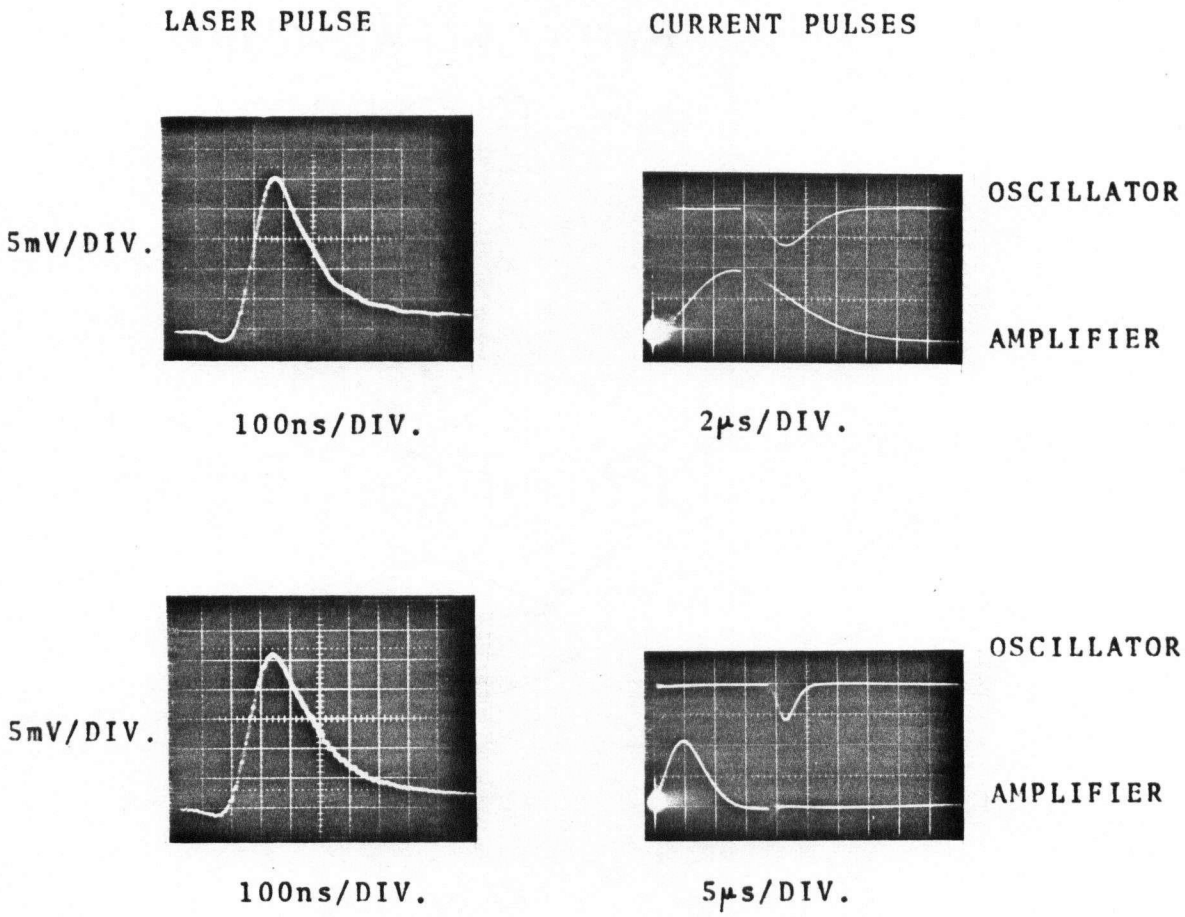

Fig. 26. The amplified laser pulse and the oscillator and amplifier current pulses are shown. The additional pump energy delivered to the active medium is seen not to increase the system gain.

The system gain was found to reach a maximum value early in the pump pulse and thereafter remain essentially constant until the termination of pumping, after which it began to fall slowly. (See Figure 27)

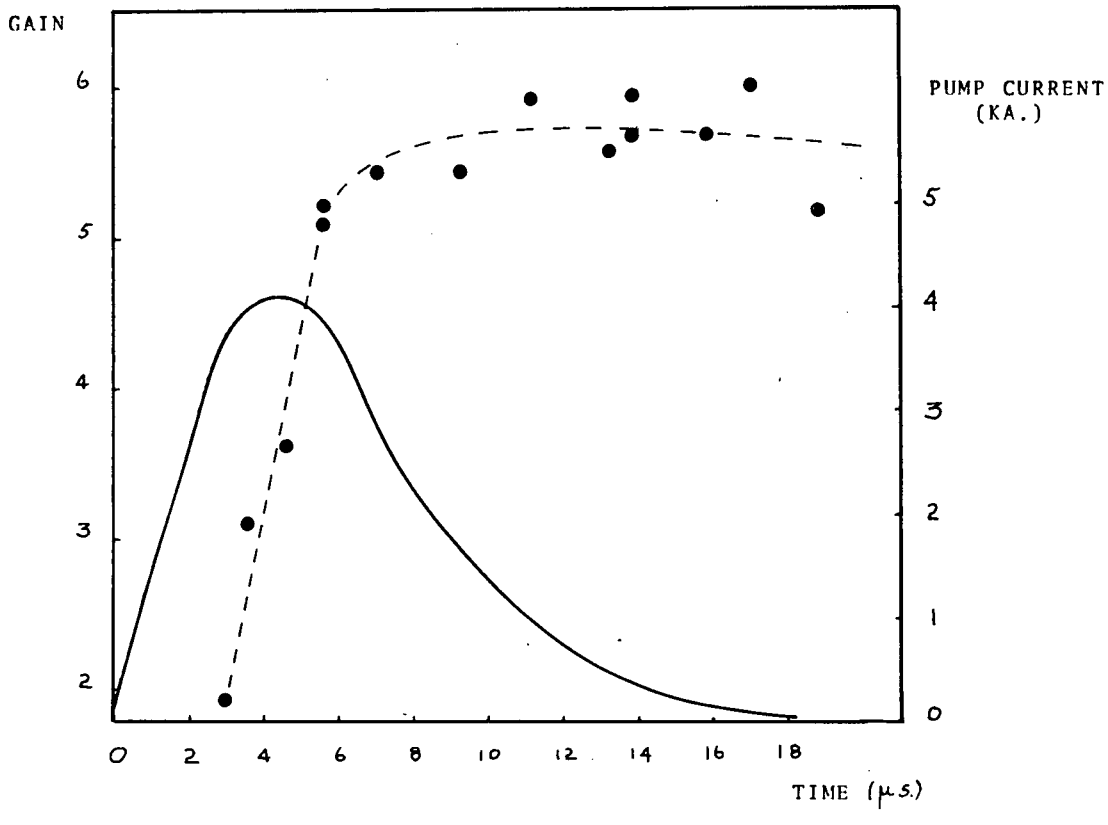

Fig. 27. The temporal behaviour of the pump current and the subsequent system gain for a zero buffer gas pressure is shown for the amplifier in its present state of construction.

This behaviour is consistent with theory which predicts that at this low pressure the inversion is quickly pumped to the threshold for parasitic oscillation and is held at this level by the radiative losses. After the pump pulse has terminated the inversion falls below this threshold and chemical deactivation slowly depletes the inversion. It was found that, contrary to theory, the addition of any buffer gas reduces the system gain. Initially, it was

believed that the buffer gas was contaminated and therefore additional chemical deactivation was occurring. However, a thorough cleaning of the gas system and a new buffer gas supply failed to eliminate the problem.

It is now believed that improper mixing of the gasses resulting in regions of high and low concentrations is the cause and in the future a mixing chamber must be used.

CHAPTER VIII CONCLUSIONS

Achievements

A gain switched oscillator and a preamplifier stage, together with the diagnostics required to monitor the performance of the entire laser and its sub-systems have been constructed and shown to function as required.

The gain of the preamplifier in its present stage of construction has been studied and has been shown to behave in accordance with theory, unless a buffer gas is added. Improper mixing of the active and buffer gasses is suggested as a reason for this discrepancy and a mixing chamber has been constructed.

Using a 20 μf capacitor bank charged to 12 KV and a zero buffer gas pressure, a maximum gain of 6 has been demonstrated. (See Figure 28)

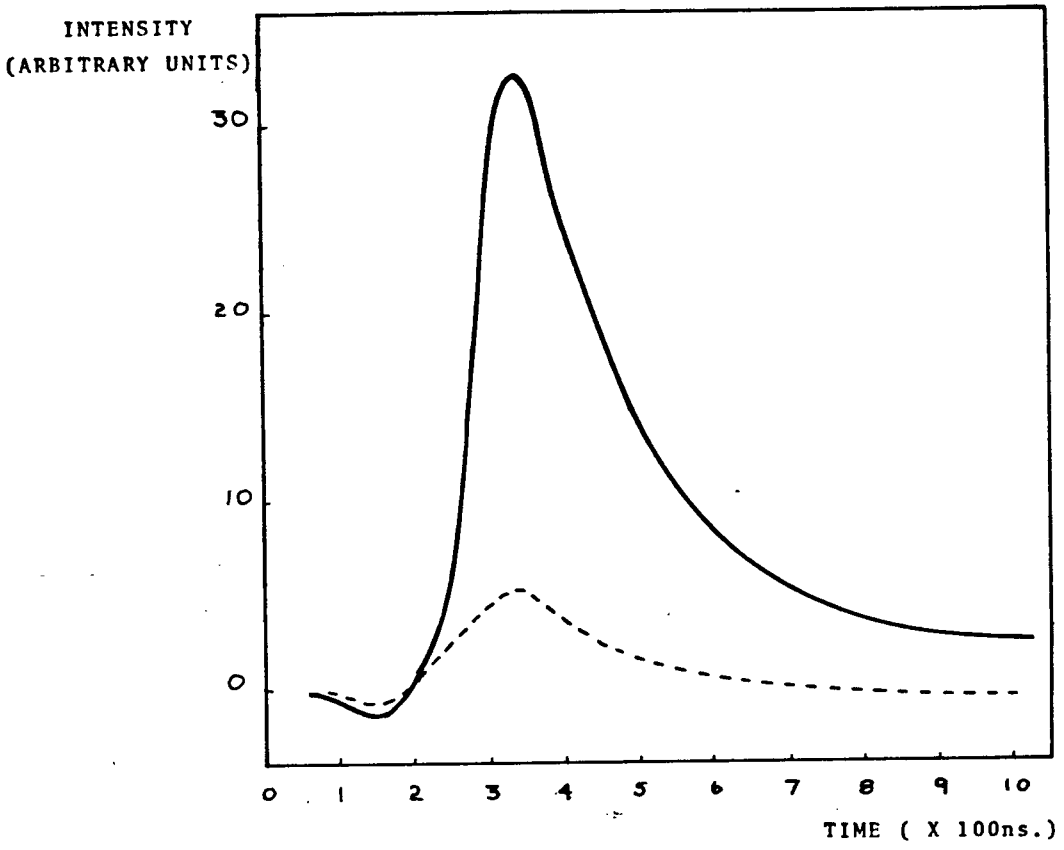

Fig. 28. The temporal profile of the intensity of the incident (broken line) and amplified (solid line) laser pulse is shown.

Suggestions for Future Work

The following suggestions are offered for the future development of the Iodine laser system at U.B.C.

The duration of the pumping pulse must be reduced or a Q switching device must be incorporated so that the energy density of the laser pulse is sufficient to achieve reasonable extraction ratios from the preamplifier stages. This improvement is particularly important

if a mode locking and a pulse cutting system are used to produce sub nanosecond pulses.

Germisil tubes must be used in place of the quartz glass laser tubes in the preamplifier stage.

Short Duration, High Power Laser Pulse
(Explosive Compression Experiments)

Active mode locking and pulse cutting systems must be included in the oscillation stage in order to generate a laser pulse of 1 ns. duration. The preamplifier stage with an active volume 1 cm. in diameter and 1 m. long, at present under construction, should be used to raise the energy of this pulse to the required 100 mJ. A final amplifier must then be designed and built to store the total energy required in the laser pulse. It must have sufficient bandwidth to accomodate the 1 ns. incident pulse.

When the construction of the oscillation and amplifier chain has been completed the operating conditions of the amplifier designed in this paper must be chosen to saturate the final amplifier. Initially, it should be operated at a pressure of 70 Torr CF_3I and 400 Torr CO_2 with a 40 μ f capacitor bank charged to 14 KV. If the incident energy at the final amplifier is above the saturation density then the changing voltage should be reduced. If not, then the incident energy should be calculated for the maximum stored energy in the capacitor bank of 6 KJ. If the saturation

energy can be achived at this higher level of stored electric energy then the lifetime of the flash tubes must be found experimentally or from data supplied by the manufacturer. The reduced flash tube lifetime may be tolerated or an additional preamplifier stage must be built to achieve the required saturation energy density of the final amplifier.

Long Duration Laser Pulse
(Ablative Compression Experiments)

The design process outlined in this paper is appropriate for an oscillator having modelocking and pulse cutting systems such that the pulse has a duration of approximately 1 ns. Without these systems the duration of the first pulse is typically 300 ns., (see figure 29) and therefore laser interaction experiments requiring long duration pulses may be performed.

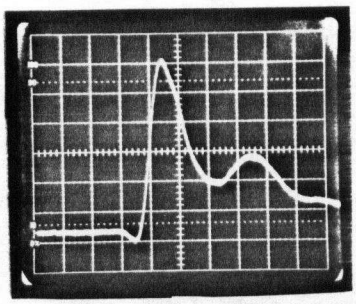

Fig. 29. A long duration laser pulse generated by a gain switched oscillator stage, without a modelocking system, is shown.

The design compromises and the operating conditions of an amplifier for long pulses are different to those required for a 1 ns. pulse. A reduced bandwidth, and consequently a lower buffer pressure, is appropriate. However, this pressure is no longer defined by the bandwidth requirement since the corresponding maximum stored energy, and hence the gain, is unreasonably small.

In this scheme the buffer gas pressure is chosen such that the small signal gain is just below the threshold value for parasitic oscillations, for a pump pulse which can be achieved reasonably easily. This contrasts with the design procedure for a sub-nanosecond pulse where the pump pulse is defined, indirectly, by the bandwidth requirement.

Thus, if in the future experiments requiring long duration laser pulses are to be performed, the preamplifier should be operated and should function as described below.

The 40 μf capacitor bank must be charged to 14 KV, thereby operating the flash tubes within the recommended limits, and the buffer gas pressure required to yield the maximum gain, found experimentally. The amplification will increase with pressure as successive parasitic modes are eliminated thereby increasing the stored energy level achieved. A further pressure increase above that required to surpress the parasitic modes will result in a reduced

amplification as the small signal gain, and hence the extraction ratio, will fall.

It is hoped that operating the oscillator stage in the high voltage regime and using the preamplifier designed in this paper to amplify the resulting long duration laser pulse will produce sufficient power to complete the evaluation of the fog cell optical isolator developed in this laboratory by B. Ahlborn, S. Ariga and D. Friedman (26). If this device proves to be successful then the design compromises necessary to achieve optical isolation will not be required and an improved laser will result.

Using an effective optical isolator, the apparatus designed in this paper could be operated as a final amplifier, thereby yielding an estimated 18 Joules in 1 ns. Useful laser-plasm interaction experiments could be performed with this 18 GW pulse.

BIBLIOGRAPHY

1. D. Porrett & C. F. Goodeve. Proc. Royal Soc. A165 31, (1938).

2. J.V.V. Kasper & G.C. Pimental. Appl. Phys. Lett. 5 231, (1964).

3. M.A. Pollack. Appl. Phys. Lett. 8, 36, (1966).

4. A.J. DeMarie & C.J. Vitee. Appl. Phys. Lett. 9, 67 (1966).

5. K. Hohla. Springer Series in Optical Sciences, Vol.9; High Power Lasers & Applications. Springer-Verlag, N.Y. (1978).

6. Laser-Fusion Research Progress Report, January-June 1976. Issued by the Directorate of Physical Research Sandia Laboratories, Alberquerque, N.M.

7. R.D. Franklin, Wright Patterson AFB, Dayton, Ohio; Technical Report, AHL 73-0071, April 1973.

8. T.L. Andreeva, S.V. Kuzretsova, A.I. Maslov, I.I. Sobel'man & V.N. Sonokin. JETP Lett. 13, 449, (1971).

9. R. G. Derwent, D. Husain & J.R. Wiesenfeld. Chem. Phys. Lett. 9, 591, (1971).

10. K. Hohla. J. Appl. Phys. 47, No. 12, 5360 (Dec. 1976).

11. V. Jaccarino et al. Phys. Rev. 94, 1798, (1954).

12. W. Fuss & K. Hohla. Max Planck Institute Fur Plasma-physik, IPP IV, 67, (1974).

13. T.D. Padnik & R.E. Palmer. J. Chem. Phys. 62, 3350, (1970).

14. R.E. Palmer, T.D. Padrik & E.D. Jones. Society of Photo-Opt. Instr. Engs. 36, 32, (1976).

15. D.W. Gregg, R.E. Kidder & C.V. Dobler. Appl. Phys. Lett. 13, 297, (1968).

16. K. Hohla. Max Planck Institute of Plasma Physics: Report No. IPP-IV/33. December, 1971.

17. G. Brederlow, K.J. Witte, E. Fill, K. Hohla & R. Volk. I.E.E.E. J. of Quant. Elec. QE-12, No. 2, 152 (1976).

18. I.M. Belousova, O.B. Danilov, I.A. Sinitsina & V.V. Sperodonov. JETP, 31, No. 5, 791 (1970).

19. E. Fill & K. Hohla. Optics. Comm. 18, No. 4, 431 (1976)

20. K. Hohla, W. Fuss, R. Volk & K.J. Witte. Optics Comm. 13, No. 2, 114, (1975).

21. K. Hohla, R. Volk, K.T. Witte. I.E.E.E. J. Quant. Elec. QE-9, 764, (1974).

22. S. Ariga & B. Ahlborn. J. Appl. Phys. 47, No. 3 (1976).

23. J.W. Olsen. J. Appl. Phys. 47, No. 12, 5360 (Dec. 1976).

24. K. Witte, G. Brederlow, E. Fill, K. Hohla & R. Volk. Laser Interaction and Related Plasma Phenomena, Vol. 4A Plenum Publising Corp. (1977).

25. J.F. Holzrichter & A.L. Schawlow. Reprint from the Annuls of the New York Academy of Sciences, Vol. 168, Article 3, pp. 703-14.

26. D. Friedman, S. Ariga & B. Ahlborn. J. Appl. Phys. 50, 5998, (1979).